International Journal of Solids and Structures 47 (2010) 1651–1665

Contents lists available at ScienceDirect

International Journal of Solids and Structures

journal homepage: www.elsevier.com/locate/ijsolstr

Much ado about shear correction factors in Timoshenko beam theory

S.B. Dong [a,*], C. Alpdogan [b], E. Taciroglu [a]

[a] Department of Civil and Environmental Engineering, University of California, Los Angeles, CA 90095, USA
[b] MMI Engineering Inc., Oakland, CA 94612, USA

ARTICLE INFO

Article history:
Received 7 January 2010
Received in revised form 23 February 2010
Available online 1 March 2010

Keywords:
Saint-Venant solutions
Semi-analytic finite elements
Shear correction factors
Timoshenko beam

ABSTRACT

Many shear correction factors have appeared since the inception of Timoshenko beam theory in 1921. While rational bases for them have been offered, there continues to be some reluctance to their full acceptance because the explanations are not totally convincing and their efficacies have not been comprehensively evaluated over a range of application. Herein, three-dimensional static and dynamic information and results for a beam of general (both symmetric and non-symmetric) cross-section are brought to bear on these issues. Only homogeneous, isotropic beams are considered. Semi-analytical finite element (SAFE) computer codes provide static and dynamic response data for our purposes. Greater clarification of issues relating to the bases for shear correction factors can be seen. Also, comparisons of numerical results with Timoshenko beam data will show the effectiveness of these factors beyond the range of application of elementary (Bernoulli–Euler) theory.

An issue concerning principal shear axes arose in the definition of shear correction factors for non-symmetric cross-sections. In this method, expressions for the shear energies of two transverse forces applied on the cross-section by beam and three-dimensional elasticity theories are equated to determine the shear correction factors. This led to the necessity for principal shear axes. We will argue against this concept and show that when two forces are applied simultaneously to a cross-section, it leads to an inconsistency. Only one force should be used at a time, and two sets of calculations are needed to establish the shear correction factors for a non-symmetrical cross-section.

1. Introduction

Timoshenko (1921, 1922) presented a beam theory involving shear correction factors to enable more accurate natural frequencies as vibrational wave lengths become shorter. Since its inception, assigning suitable factors to various cross-sections have occupied the attention of many investigators. The most recent methods for devising these factors rest on some form of static or dynamic data from linear three-dimensional elasticity. While many rational methods have been proposed, lingering thoughts remain. Is there a most suitable method for selecting them? What is their effectiveness for more accurate modeling of physical behavior beyond the range of classical beam theory? We strive to provide clarifying discussions to these questions. Our response is based on having three-dimensional elastostatic and elastodynamic data for prismatic beams of any cross-section. Clearly, such data will enable any beam theory to be assessed over any range of application.

The three-dimensional beam data herein are found by means of a semi-analytical finite element (SAFE) method so that any cross-sectional shape can be modeled. In this SAFE formulation, only the cross-section undergoes discretization – i.e., in the (x,y) plane – while both time t and axial dependence z are treated analytically, see Fig. 1. The governing equations of motion have the form

$$\mathbf{K_1}\mathbf{U}_{,zz} - \mathbf{K_2}\mathbf{U}_{,z} - \mathbf{K_3}\mathbf{U} - \mathbf{M}\ddot{\mathbf{U}} = \mathbf{F}, \tag{1}$$

where $\mathbf{U}(z,t)$ and $\mathbf{F}(z,t)$ of length $3M$ are assemblages of nodal displacements and consistent loads for the M nodes of the finite element mesh, i.e.,

$$\mathbf{U}^T(z,t) = [\cup\mathbf{u}(z,t) \cup \mathbf{v}(z,t), \cup\mathbf{w}(z,t)] \quad \mathbf{F}^T = [\cup\mathbf{f_x}, \cup\mathbf{f_y}, \cup\mathbf{f_z}]. \tag{2}$$

System matrices $\mathbf{K_1}$, $\mathbf{K_2}$, $\mathbf{K_3}$, and $\mathbf{M}$ are found in Taweel et al. (2000). Standard isoparametric methodology was used where both six-node triangles and eight-node quads (i.e., quadratic interpolation fields) were provided for modeling of the cross-section. Appropriate forms of Eq. (1) together with Ieşan's method (1976,1986,1987) for setting forth the appropriate displacement fields were used for Saint-Venant and Almamsi-Michell solutions by Dong et al. (2001), Kosmatka et al. (2001) and Lin and Dong (2006). The homogeneous form of Eq. (1) was used for free vibration results by Taweel et al. (2000).

There is a rather extensive extant literature on finite element analyses of Saint-Venant's flexure, viz., Mason and Herrmann (1968), Tolf (1985), Wörndle (1982), Giavotto et al. (1983), Kosmatka and Dong (1991), Schramm et al. (1994), Popescu and

* Corresponding author. Tel.: +1 310 825 5353.
E-mail address: dong@seas.ucla.edu (S.B. Dong).

0020-7683/$ - see front matter © 2010 Elsevier Ltd. All rights reserved.
doi:10.1016/j.ijsolstr.2010.02.018

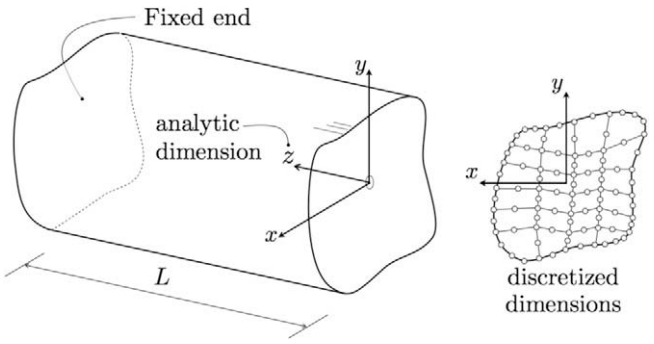

Fig. 1. Problem geometry and its semi-analytical finite element discretization.

Hodges (2000), Gruttmann and Wagner (2001), Ladevéze et al. (2001), El Fatmi and Zenzri (2002, 2004), and El Fatmi (2007a,b). The SAFE method was preferred, because of its ease in displaying displacement results. In solutions employing the semi-inverse method involving a stress function, the displacements can be determined only after the stress state is established. Such displacement data are quite often not shown. We will see the advantages of visual display of the displacement field in explaining the effect of shear. We note that the methods of El Fatmi and Zenzri (2002, 2004) and El Fatmi (2007a,b) are closely akin to the SAFE formulation. Their analyses are based on Ladevéze and Simmonds (1998) and displacement data were easily showcased.

Cowper (1966) was the first to use Saint-Venant flexure (i.e., three-dimensional) data to set forth shear correction factors. His procedure involves integration of three-dimensional elasticity equations to form beam-type deformations, constitutive relations and equations of equilibrium. It ultimately led to integration of shear warpage of Saint-Venant flexure solution to peg the shear correction factor in the shear constitutive relation. Cowper dealt with homogeneous, isotropic symmetric cross-sections. Mason and Herrmann (1968) generalized Cowper's procedure for general homogeneous, isotropic cross-sections, wherein they determine the shear warpage by finite element analysis. Gruttmann and Wagner (2001) presented additional results, which essentially followed Mason and Hermann's methodology. We will show that integration of the SAFE warpage field at the root end of a cantilevered beam yields a weighted-average shear angle. This shear angle is directly related to the shear correction factor. Moreover, these factors have the same magnitude as that of Cowper (1966) and Mason and Herrmann (1968). The correction for shear deflection on this basis shows the deflection curve of the centroidal axis by three-dimensional and Timoshenko theories to be in agreement over the entire length of a beam.

Other elastostatic approaches for shear correction factors will also be discussed. One prominent method is due to Renton (1991), who related the Timoshenko beam correction factors to the transverse shear strain energy per unit length of beam, which is constant for a beam in flexure. In our evaluation of correction factors for rectangular and elliptical cross-sections with extremely flat aspect ratios, very low values were found, which immediately raised doubts on their efficacy. A modification is suggested, where only energy due to the shear stress component in the direction of transverse force is used. Numerical results are given to test this suggestion. Schramm et al. (1994) adopted Renton's approach for general cross-sections. In their paper, they suggested the existence of principal shear axes which did not coincide with the principal bending axes. In another elastostatic approach, Popescu and Hodges (2000) used a variational-asymptotic method due to Berdichevsky and Starosel'skii (1983) to formulate an elasticity solution. The data from this analysis was used to determine shear correction factors for anisotropic beams. Their example on homogeneous, isotropic cross-sections corroborated those of Renton and Schramm et al. (1994). We will argue that the concept of principal shear axes independent of principal bending axes is not viable.

Shear correction factors from free vibration data are also considered. Mindlin and Deresiewicz (1954) pegged the correction factors to frequencies of the lowest mode of infinitely long thickness-shear vibration by three-dimensional theory. This method is the extension of Mindlin (1951)'s well known shear deformation theory for homogeneous, isotropic plates.[1] Mindlin and Deresiewicz (1954) provided data for rectangular, circular, elliptical and ovaloidal cross-sections. In a recent paper, Hutchinson (2001) suggested another method using a Hellinger–Reissner variational theorem to derive "best" possible beam equations of motion that accounts for shear deformation. His method is based on independent assumptions of stress and displacement fields. Upon comparison of his solutions with that of conventional Timoshenko beam equations, formulas for shear correction factors are established. Hutchinson's dealt only with symmetric cross-sections. By and large, the vibration approach has received markedly less attention due to lack of three-dimensional data by which to assess Timoshenko beam results. With the SAFE approach where such data are easily generated, this is not an issue.

In this paper, we employ rectangular Cartesian coordinates (x,y,z) throughout, with the z axis coinciding with the line of centroids of the cross-section. The (x,y) axes are always taken to be parallel to the principal bending directions. For elastostatic problems, a cantilever beam is involved; the origin of coordinates is situated at the tip end of the beam and the z-axis runs toward the root end. For elastodynamics, sinusoidal waves travel along the z-direction so that the beam is assumed to be infinite in extent. With the use of principal bending axes, two correction factors in the principal directions can be determined for two uncoupled shear constitutive relations. Then, constitutive relations in any other coordinate system are possible by transformation equations of a two-dimensional second rank tensor.

2. Synopsis of the Timoshenko beam equations

Herein, we summarize the equations for Timoshenko beam theory. Let $u(z,t)$ and $v(z,t)$ be components of the deflection of the centroidal axis, and $\beta_x(z,t)$ and $\beta_y(z,t)$ as the bending rotations about the (x,y) axes, respectively. The slopes to the deflection curve are

$$\frac{\partial u}{\partial z} = \beta_y + \gamma_x, \quad \frac{\partial v}{\partial z} = \beta_x + \gamma_y, \tag{3}$$

where $\gamma_x(z,t)$ and $\gamma_y(z,t)$ are the shear angles. The constitutive equations relating these kinematic variables to moments and shears, (M_x, M_y, V_x, V_y), are

$$\begin{aligned} M_x &= -EI_{xx}\frac{\partial \beta_x}{\partial z}, \quad V_y = k_{22}^2 GA\gamma_y = k_{22}^2 GA\left\{\frac{\partial v}{\partial z} - \beta_x\right\} \\ M_y &= -EI_{yy}\frac{\partial \beta_y}{\partial z}, \quad V_x = k_{11}^2 GA\gamma_x = k_{11}^2 GA\left\{\frac{\partial u}{\partial z} - \beta_y\right\}, \end{aligned} \tag{4}$$

where E, G are the extensional and shear moduli, A the cross-sectional area, and I_{xx}, I_{yy} the planar moments of inertia. Coefficients k_{11}^2 and k_{22}^2 are shear correction factors. It is well established that the flexural rigidities of the moment–curvature relations submit to transformation as a second rank tensor with rotation of the coordinate system about the z-axis. The transverse shear rigidities (i.e., the correction factors) will also abide by this transformation, as they are components of a second rank tensor. The principal shear

[1] The analogue elastostatics approach is due to Reissner (1945, 1947).

rigidity data allow data in any other coordinate system to be found by a rotation about the z-axis.

The transverse and rotational equations of motion are

$$\begin{aligned} &\frac{\partial V_x}{\partial z}+p_x=\rho A\ddot{u}, \quad \frac{\partial M_y}{\partial z}-V_x=\rho I_{yy}\ddot{\beta}_y,\\ &\frac{\partial V_y}{\partial z}+p_y=\rho A\ddot{v}, \quad \frac{\partial M_x}{\partial z}-V_y=\rho I_{xx}\ddot{\beta}_x, \end{aligned} \tag{5}$$

where ρ is the unit mass density and p_x and p_y are transverse loads. Substitution of constitutive relations (4) into Eq. (5) yields the kinematic equations of motion:

$$\begin{aligned} &k_{11}^2GA\left\{\frac{\partial^2 u}{\partial z^2}-\frac{\partial \beta_y}{\partial z}\right\}+p_x=\rho A\ddot{u},\\ &EI_{yy}\frac{\partial^2\beta_y}{\partial z^2}+k_{11}^2GA\left\{\frac{\partial u}{\partial z}-\beta_y\right\}=-\rho I_{yy}\ddot{\beta}_y,\\ &k_{22}^2GA\left\{\frac{\partial^2 v}{\partial z^2}-\frac{\partial \beta_x}{\partial z}\right\}+p_y=\rho A\ddot{v},\\ &EI_{xx}\frac{\partial^2\beta_x}{\partial z^2}+k_{22}^2GA\left\{\frac{\partial v}{\partial z}-\beta_x\right\}=-\rho I_{xx}\ddot{\beta}_x. \end{aligned} \tag{6}$$

Boundary conditions at an end $z=z_o$ are in terms of prescribed displacement or shear and prescribed rotation or moment.

$$\begin{aligned} &u(z_o,t)=\bar{u}, \text{ or } V_x(z_o,t)=\overline{V}_x \quad \text{and}\\ &\quad v(z_o,t)=\bar{v}, \text{ or } V_y(z_o,t)=\overline{V}_y \end{aligned} \tag{7a}$$

$$\begin{aligned} &\beta_x(z_o,t)=\bar{\beta}, \text{ or } M_x(z_o,t)=\overline{M}_x \quad \text{and}\\ &\quad \beta_y(z_o,t)=\bar{\beta}, \text{ or } M_y(z_o,t)=\overline{M}_y, \end{aligned} \tag{7b}$$

where an overbar denotes a prescribed condition.

3. Shear correction factors based on Saint-Venant flexure

In Fig. 1, the Cartesian coordinate system is shown where the origin is located at the centroid of the *tip* end of the beam with the z-axis running toward the *root* end. The (x,y) axes in any generic cross-section coincide with the principal bending axes. Saint-Venant flexure consists of determining the three-dimensional stress and displacement fields in a prismatic beam of length L subjected to prescribed shear tractions at the tip end whose resultants are P_x and P_y and full restraint at the root end. What is known as Saint-Venant's solution consists of a stress field, which agrees only in terms of the transverse resultant magnitudes for P_x and P_y, but not necessarily on a point-wise traction basis. At the root end, a complete point-wise kinematic restraint is relaxed and the following conditions at the centroid are usually enforced:

$$\begin{aligned} &u(0,0,L)=0, \quad v(0,0,L)=0, \quad w(0,0,L)=0,\\ &\frac{\partial u(0,0,L)}{\partial z}=0, \quad \frac{\partial v(0,0,L)}{\partial z}=0, \quad \frac{\partial v(0,0,L)}{\partial x}-\frac{\partial u(0,0,L)}{\partial y}=0. \end{aligned} \tag{8}$$

The SAFE methodology of Dong et al. (2001) consists of setting forth the Saint-Venant flexure displacement field at the outset. This field and those for the Almansi–Michell problems are available via Ieşan's procedure (1986) of sequential integration, beginning with a rigid body field. The flexure field is composed of three parts: (1) primal field, (2) cross-sectional warpage and (3) rigid body motion, all of which are associated with unknown displacement coefficients.

$$\begin{aligned} u(x,y,z)=&-a_{II5}\frac{z^3}{6}-a_{II6}\frac{yz^2}{2}-a_{I5}\frac{z^2}{2}-a_{I6}yz\\ &+a_{II3}\{z\psi_{I3u}+\psi_{II3u}\}+a_{II4}\{z\psi_{I4u}+\psi_{II4u}\}\\ &+a_{II5}\{z\psi_{I5u}+\psi_{II5u}\}+a_{II6}\{z\psi_{I6u}+\psi_{II6u}\}\\ &+a_{I3}\psi_{I3u}+a_{I4}\psi_{I4u}+a_{I5}\psi_{I5u}\\ &+a_{I6}\psi_{I6u}-\omega_3y-\omega_2z+u_o \end{aligned}$$

$$\begin{aligned} v(x,y,z)=&-a_{II4}\frac{z^3}{6}+a_{II6}\frac{xz^2}{2}-a_{I4}\frac{z^2}{2}+a_{I6}xz\\ &+a_{II3}\{z\psi_{I3v}+\psi_{II3v}\}+a_{II4}\{z\psi_{I4v}+\psi_{II4v}\}\\ &+a_{II5}\{z\psi_{I5v}+\psi_{II5v}\}+a_{II6}\{z\psi_{I6v}+\psi_{II6v}\}\\ &+a_{I3}\psi_{I3v}+a_{I4}\psi_{I4v}+a_{I5}\psi_{I5v}\\ &+a_{I6}\psi_{I6v}+\omega_3x-\omega_1z+v_o \end{aligned}$$

$$\begin{aligned} w(x,y,z)=&\frac{1}{2}(a_{II3}+a_{II5}x+a_{II4}y)z^2\\ &+(a_{I3}+a_{I5}x+a_{I4}y)z+a_{II3}\{z\psi_{I3w}+\psi_{II3w}\}\\ &+a_{II4}\{z\psi_{I4w}+\psi_{II4w}\}+a_{II5}\{z\psi_{I5w}+\psi_{II5w}\}\\ &+a_{II6}\{z\psi_{I6w}+\psi_{II6w}\}+a_{I3}\psi_{I3w}+a_{I4}\psi_{I4w}\\ &+a_{I5}\psi_{I5w}+a_{I6}\psi_{I6w}+\omega_1y+\omega_2x+w_o, \end{aligned} \tag{9a}$$

where all the warpages, ψ_I's and ψ_{II}'s, are functions of (x,y) only. Recasting Eq. (9a) in matrix form yields

$$\mathbf{U}(z)=\underset{3M\times 4}{\left[\mathbf{\Phi_{sv2}}(z)+z\mathbf{\Psi_{sv1}}+\mathbf{\Psi_{sv2}}\right]}\underset{4\times 1}{\mathbf{a_I}}+\underset{3M\times 4}{\left[\mathbf{\Phi_{sv1}}(z)+\mathbf{\Psi_{sv1}}\right]}\underset{4\times 1}{\mathbf{a_I}}+\underset{3M\times 6}{\mathbf{\Phi_{RB6}}(z)}\underset{6\times 1}{\mathbf{a_{RB6}}}, \tag{9b}$$

where the entries in $\mathbf{a_I}$, $\mathbf{a_{II}}$, $\mathbf{a_{RB6}}$ are unknown kinematic coefficients given by

$$\begin{aligned} &\mathbf{a_I}=[a_{I3},a_{I4},a_{I5},a_{I6}]^T, \quad \mathbf{a_{II}}=[a_{II3},a_{II4},a_{II5},a_{II6}]^T,\\ &\mathbf{a_{RB6}}=[u_o,v_o,w_o,\omega_1,\omega_2,\omega_3]^T; \end{aligned} \tag{10}$$

and $(\mathbf{\Phi_{sv1}},\mathbf{\Phi_{sv2}})$ and $(\mathbf{\Psi_{sv1}},\mathbf{\Psi_{sv2}})$ are the primal fields and warpages for extension–bending–torsion ($sv1$) and flexure ($sv2$), respectively; and $\mathbf{\Phi_{RB6}}$ contain six unit rigid body displacement components. Note that the warpages $(\mathbf{\Psi_{sv1}},\mathbf{\Psi_{sv2}})$ are independent of z, and $\mathbf{\Phi_{RB6}}$ can be stated by inspection.

The primal fields $(\mathbf{\Phi_{sv1}},\mathbf{\Phi_{sv2}})$ are given by Ieşan's procedure (1986). The warpages $(\mathbf{\Psi_{sv1}},\mathbf{\Psi_{sv2}})$ are found by substitution of displacement field (9) into Eq. (1) in which the load and inertial terms have been suppressed. The details in this step can be found in Dong et al. (2001). Once these warpages have been established, the stress distribution can be written as

$$\boldsymbol{\sigma}=[z\boldsymbol{\sigma}_0+\boldsymbol{\sigma}_1]\mathbf{a_{II}}+\boldsymbol{\sigma}_0\mathbf{a_I} \text{ where } \begin{cases}\boldsymbol{\sigma}_0=\mathbf{C}[\mathbf{h}+\mathbf{b_1}\boldsymbol{\psi}_{sv1_i}]\mathbf{a_I}\\ \boldsymbol{\sigma}_1=\mathbf{C}[\mathbf{b_2}\boldsymbol{\psi}_{sv1_i}+\mathbf{b_1}\boldsymbol{\psi}_{sv2_i}]\mathbf{a_{II}}\end{cases}, \tag{11}$$

where $\mathbf{b_1}$, $\mathbf{b_2}$ are strain-transformation equations – see, Taweel et al. (2000) – and $\mathbf{h}$ is

$$\mathbf{h}=\begin{bmatrix} \cdot & \cdot & \cdot & \cdot & \cdot & \cdot\\ \cdot & \cdot & \cdot & \cdot & \cdot & \cdot\\ \cdot & \cdot & 1 & y & x & \cdot\\ \cdot & 1 & \cdot & \cdot & \cdot & x\\ 1 & \cdot & \cdot & \cdot & \cdot & -y\\ \cdot & \cdot & \cdot & \cdot & \cdot & \cdot \end{bmatrix}. \tag{12}$$

Integrating stress components $(\sigma_{zz},\ \sigma_{zy},\ \sigma_{zx})$ over a generic cross-section Π at station z yields the force and moment resultants (P_z,M_x,M_y,M_z):

$$\mathbf{F}(z)\equiv\begin{Bmatrix}P_z(z)\\M_x(z)\\M_y(z)\\M_z(z)\end{Bmatrix}=\int\int_{\Pi}\begin{Bmatrix}\sigma_{zz}\\ \sigma_{zz}y\\ \sigma_{zz}x\\ \sigma_{zy}x-\sigma_{zx}y\end{Bmatrix}dxdy. \tag{13}$$

For Saint-Venant flexure, vector $\mathbf{F}(z)$ at any cross-section is given by,

$$\mathbf{F}(z) = z\begin{Bmatrix} \cdot \\ P_y \\ -P_x \\ \cdot \end{Bmatrix} + \begin{Bmatrix} \cdot \\ \cdot \\ \cdot \\ P_y e_x + P_x e_y \end{Bmatrix}, \tag{14}$$

where P_x and P_y are the transverse forces, and e_x and e_y are distances to the shear center. This form of $\mathbf{F}(z)$ satisfies global equilibrium. Torque $M_z(z)$ involving e_x and e_y occurs only if the centroid and shear center are not coincident. Carrying out the integration in Eq. (13), and setting this result equal to Eq. (14) give

$$\begin{bmatrix} EA & \cdot & \cdot & \cdot \\ \cdot & EI_{xx} & \cdot & \cdot \\ \cdot & \cdot & EI_{yy} & \cdot \\ \cdot & \cdot & \cdot & GJ \end{bmatrix} \left[z\begin{Bmatrix} a_{II3} \\ a_{II4} \\ a_{II5} \\ a_{II6} \end{Bmatrix} + \begin{Bmatrix} a_{I3} \\ a_{I4} \\ a_{I5} \\ a_{I6} \end{Bmatrix} \right] + \begin{bmatrix} \kappa_{II33} & \kappa_{II34} & \kappa_{II35} & \kappa_{II36} \\ \kappa_{II43} & \kappa_{II44} & \kappa_{II45} & \kappa_{II46} \\ \kappa_{II53} & \kappa_{II54} & \kappa_{II55} & \kappa_{II56} \\ \kappa_{II63} & \kappa_{II64} & \kappa_{II65} & \kappa_{II66} \end{bmatrix} \begin{Bmatrix} a_{II3} \\ a_{II4} \\ a_{II5} \\ a_{II6} \end{Bmatrix} = z\begin{Bmatrix} \cdot \\ P_y \\ -P_x \\ \cdot \end{Bmatrix} + \begin{Bmatrix} \cdot \\ \cdot \\ \cdot \\ P_y e_x + P_x e_y \end{Bmatrix}, \tag{15}$$

where EA, EI_{xx}, EI_{yy}, GJ are extensional, flexural and torsional rigidities of the cross-section. For a homogeneous isotropic beam, the second term on the left-hand side of this equation involving $\boldsymbol{\kappa}_{II}$ is zero. To determine $\mathbf{a}_{II}$, differentiate Eq. (15) with respect to z, which leads to

$$\begin{bmatrix} EA & \cdot & \cdot & \cdot \\ \cdot & EI_{xx} & \cdot & \cdot \\ \cdot & \cdot & EI_{yy} & \cdot \\ \cdot & \cdot & \cdot & GJ \end{bmatrix} \begin{Bmatrix} a_{II3} \\ a_{II4} \\ a_{II5} \\ a_{II6} \end{Bmatrix} = \begin{Bmatrix} \cdot \\ P_y \\ -P_x \\ \cdot \end{Bmatrix} \rightarrow \begin{Bmatrix} a_{II3} \\ a_{II4} \\ a_{II5} \\ a_{II6} \end{Bmatrix} = \begin{Bmatrix} \cdot \\ P_y/EI_{xx} \\ -P_x/EI_{yy} \\ \cdot \end{Bmatrix}. \tag{16}$$

Coefficients in $\mathbf{a}_{I}$ are then found by setting $z = 0$ in Eq. (15). All coefficients are equal to zero except for a_{I6}, and it will only appear when the shear center does not coincide with the centroid. At this stage of the analysis, note that the stress state is uniquely determined. The final step in the analysis is the evaluation of rigid body displacements $\mathbf{a}_{RB6}$ from restraint conditions (8), which yields

$$u_0 = -P_x L^3/6EI_{yy}, \quad v_0 = P_y L^3/6EI_{xx}, \quad w_0 = 0,$$
$$\omega_1 = P_y L^2/2EI_{xx}, \quad \omega_2 = -P_x L^2/2EI_{yy}, \quad \omega_3 = -\frac{L}{GJ}(P_y e_x - P_x e_y). \tag{17}$$

Once displacement field (9) is established, we can examine it to observe the effect of shear. Consider a unit transverse load, say $P_y = 1$. The centerline deflection is given by Eq. (9)[2] with $x = y = 0$:

$$v(0,0,z)|_{P_y=1} = \frac{1}{6EI_{xx}}(z^3 - 3L^2 z + 2L^3), \quad \text{and} \quad v(0,0,0)|_{P_y=1} = \frac{L^3}{3EI_{xx}}. \tag{18}$$

This deflection curve is the same as that in Bernoulli–Euler theory. Boundary conditions (8) giving rigid body components (17) enable the Saint-Venant centroidal deflection to match that of Bernoulli–Euler beam theory. Then, how does transverse shear deformation evince itself? It is embodied in the out-of-plane warpage function $\psi_{II4w}(x,y)$, an effect that is independent of the length of the beam. This warpage by itself can be seen at the root end because, at that cross-section, the Saint-Venant displacement field is free from all effects due to the primal field and rigid body displacements. Examples of such warpages for the various cross-sections are shown in Fig. 2 for cross-sections that will be discussed later on. The arrow indicate the direction of the transverse force. Similar plots are seen in El Fatmi and Zenzri (2004) and El Fatmi (2007b). A related plot is seen in Timoshenko and Goodier (1970, pp. 44–45) in connection with their plane-strain analysis of flexure. From these plots, it is obvious that the relaxed boundary conditions of Eq. (8) do not result in full axial restraint at the root end.

The Saint-Venant flexure solution is unique to within a rigid body displacement. The root-end shear effect, as illustrated in Fig. 2, can be approximated by an angle γ_y (a weighted-average value) that replaces warpage $\psi_{II4w}(x,y)$.

$$\psi_{II4w}(x,y)|_{P_y} \approx \gamma_y y. \tag{19}$$

Incorporating γ_y in the Saint-Venant flexure solution as a rigid body rotation will restore the root end to its original (undeformed) configuration on an average basis. Moreover, when this rotation is multiplied by distance with the root end, the entire centroidal deflection is corrected for shear. To determine γ_y, multiply both sides by y and integrate.[3]

$$\int\int [\psi_{II4w}(x,y)|_{P_y}] y dA = \gamma_y \int\int y^2 dA = \gamma_y I_{xx} \tag{20a}$$

or

$$\gamma_y = \frac{1}{I_{xx}} \int\int [\psi_{II4w}(x,y)|_{P_y}] y \, dx \, dy. \tag{20b}$$

From shear constitutive relation (4) for a unit force P_y, $\gamma_y = 1/k_{22}^2 GA$. Therefore, the shear correction factor emerges as

$$\frac{1}{k_{22}^2} = \frac{GA}{I_{xx}} \int\int y[\psi_{II4w}(x,y)|_{P_y}] \, dx \, dy. \tag{21}$$

By a similar calculation, the shear correction factor in the other principal direction is

$$\frac{1}{k_{11}^2} = \frac{GA}{I_{yy}} \int\int x[\psi_{II5w}(x,y)|_{P_x}] \, dx \, dy. \tag{22}$$

Herein, the values of the shear correction factors are calculated by Gaussian quadrature of the SAFE Saint-Venant results. Recall that they were predicated on quadratic polynomial displacement interpolations over the cross-section. In formulas (21) and (22), shear modulus G appears; however, it should be remembered that functions $\psi_{II4w}(x,y)$ and $\psi_{II5w}(x,y)$ also involve a similar factor in them so that k_{11}^2 and k_{22}^2 are ultimately independent of this material parameter. Lastly, we note that the residual out-of-plane warpage (the difference between ψ_{II4w} and average displacement $y\gamma_y$) is a displacement field of a self-equilibrated state. According to Saint-Venant's principle, it decays with distance from the root end, where the decay distance can be quantified, see Lin et al. (2001) and Alpdogan et al. (2010).

In our examples, the shear correction factors by Eqs. (21) and (22) agree with those of Cowper (1966) and Mason and Herrmann (1968). Cowper's method used data based on a semi-inverse method (stress function) of solution to derive the shear constitutive relation, so that the displacement field was not directly involved. While Mason and Herrmann did solved for the out-of-plane warpages for general cross-sections, they utilized these data in the same way as Cowper. We can therefore conclude that their methods for shear correction factors correspond to our characterization

[2] All warpage functions at the centroid of the displacement field can be set equal to zero since they are unique only to within a rigid body motion of three translations and a rotation about the z-axis.

[3] Integrating both sides of Eq. (19) without multiplying by y will result in the right-hand side vanishing as the origin is located at the centroid, i.e., $\int y dA = 0$.

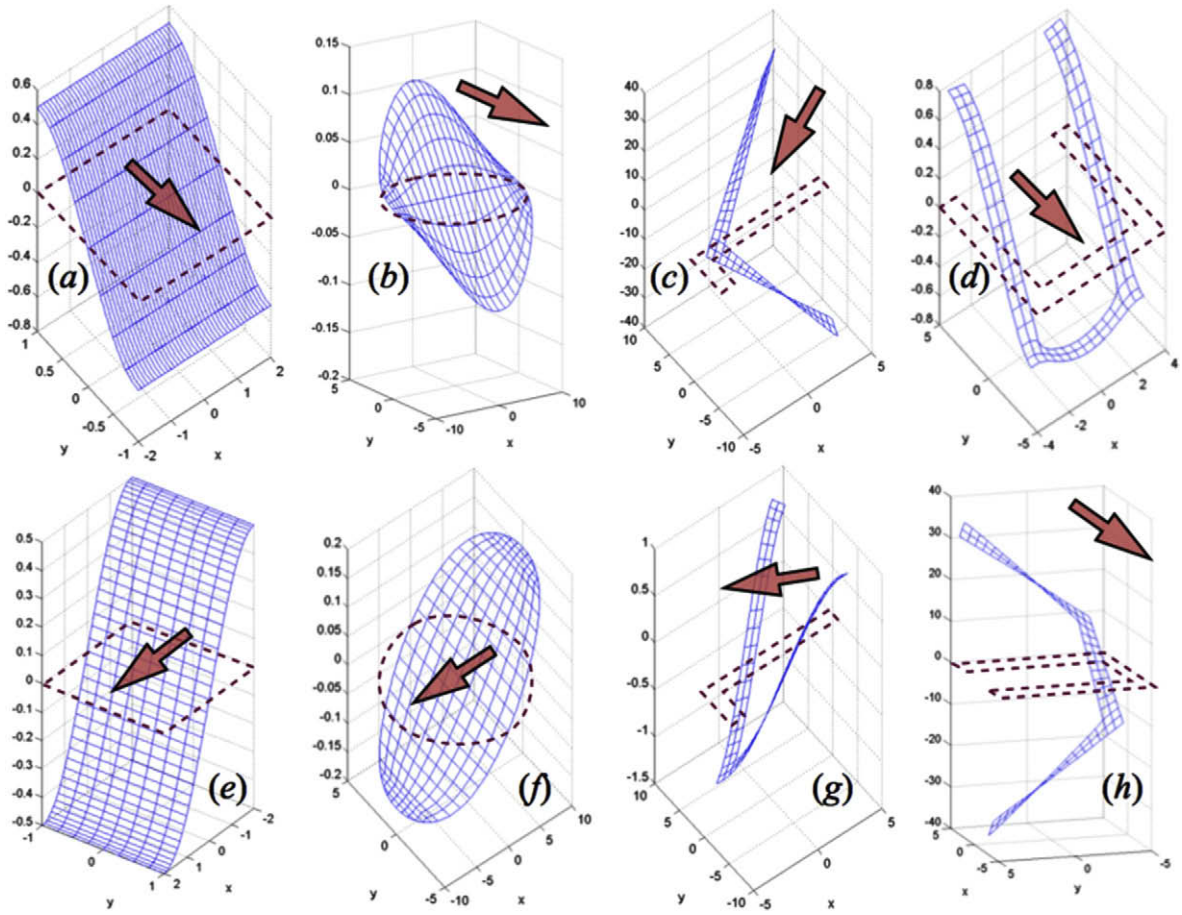

Fig. 2. Examples of Saint-Venant warpages at the root-end of beams: (a, e) Rectangle sections with aspect ratios of 2 or 0.5; (b, f) ellipse sections with aspect ratio of 2 and 0.5; (c, g) angle section No. 1, and (d, h) channel section No. 1.

of them as weighted-average values. A correction for shear is one that returns the root-end cross-section to its original configuration, albeit on an average basis, by a rigid body rotation about a principal bending axis. The Saint-Venant centroidal deflection given by Eq. (18) and augmented with a correction for shear becomes

$$v(0,0,z)|_{P_y=1} = \frac{1}{6EI_{xx}}(z^3 - 3L^2z + 2L^3) + \frac{1}{k_{22}^2 GA}(L - z). \tag{23}$$

This expression is the same as that by the Timoshenko beam equations. Thus, we have a very compelling reason to regard the shear correction factors of Cowper (1966) and Mason and Herrmann (1968) as the most effective (at least for tip loaded cantilevered beams). Their coefficients produce a deflection curve that tracks the three-dimensional elasticity curve over the entire centroidal axis.

Renton (1991) presented a method for shear correction factors based on energy of transverse shear stresses, which is uniform along the centroidal axis for a tip loaded cantilevered beam. He evaluated this energy using the Saint-Venant flexure data, i.e.,

$$U_{s-total} = \frac{G}{2}\int\int_A (\gamma_{xz}^2 + \gamma_{yz}^2)dA \tag{24}$$

and equated it to an equivalent expression based on Timoshenko beam theory. For example, for shear force V_y, the equivalent shear energy W_{Timo}, in terms of K_y (shear stiffness of the beam), is

$$W_{Timo} = \frac{1}{2}\frac{V_y^2}{K_y} \qquad \text{where} \quad K_y = k_{22}^2 GA. \tag{25}$$

Thus, the correction factor can be determined. Renton dealt with symmetric cross-sections only.

In our examples on rectangular and elliptical cross-sections, we found that Renton's method gave quite low shear correction values for extremely flat cross-sections. We have included another energy version, where only the transverse shear energy of shear strain in the direction of the force is used – the rationale being that only such deformation contributes to a net shear deflection. For example, for a transverse force in the y-direction, the energy is

$$U_{s-directional} = \frac{G}{2}\int\int_A \gamma_{yz}^2\, dA. \tag{26}$$

Equating this expression to that given by Eq. (25) yields another correction factor. We shall call this version the *directional shear energy* method and test its efficacy along with all other correction factors considered herein.

4. Shear correction factors based on free vibration data

The method for shear correction factors on a dynamic basis is due to Mindlin and Deresiewicz (1954). It follows the concept for plates by Mindlin (1950), where the lowest thickness-shear frequency from three-dimensional elasticity is utilized. The governing equation for free vibration is the homogeneous form of Eq. (1), from which the frequencies of harmonic propagating waves in the z-direction are sought. The solution form for harmonic waves is

$$\mathbf{U}(z,t) = \mathbf{U_o} e^{i(kz-\omega t)}, \tag{27}$$

where k is an axial wave number related to wavelength λ by $k = \pi/\lambda$, and ω is the natural frequency. Substituting this solution form into the homogeneous form of Eq. (1) yields

$$k^2\mathbf{K_1U_o} + ik\mathbf{K_2U_o} + \mathbf{K_3U_o} = \omega^2\mathbf{MU_o}. \tag{28a}$$

As $\mathbf{K_1}$, $\mathbf{K_3}$ and $\mathbf{M}$ are symmetric and $\mathbf{K_2}$ is antisymmetric, this complex equation is hermitian. It can be rendered into a real symmetric positive semi-definite system by doubling the matrix rank, as in,

$$\begin{bmatrix} \mathbf{K_3} + k^2\mathbf{K_1} & -k\mathbf{K_2} \\ k\mathbf{K_2} & \mathbf{K_3} + k^2\mathbf{K_1} \end{bmatrix} \begin{Bmatrix} \mathbf{U_o} \\ -i\mathbf{U_o} \end{Bmatrix} = \omega^2 \begin{bmatrix} \mathbf{M} & \cdot \\ \cdot & \mathbf{M} \end{bmatrix} \begin{Bmatrix} \mathbf{U_o} \\ -i\mathbf{U_o} \end{Bmatrix}. \tag{28b}$$

The roots for ω^2 of Eq. (28b) are real and repeated. Each pair of repeated roots corresponds to propagating waves of the same wave number k but traveling in the opposite directions. The eigendata from this system provide spectral data for all possible waves that can occur in the beam. They include the axial, flexural and torsional modes as the lowest branches, followed by thickness-shear and thickness-stretch modes, and then of all of the higher branches. In our discussion, we will only be concerned with the flexural and thickness-shear branches in this spectra.

The governing equations for free vibration in Timoshenko theory are those in Eq. (6). The analogous expressions for infinite trains of sinusoidal waves in the x–z and y–z planes are

$$\begin{aligned} u(x,t) &= Ue^{i(kz-\omega t)}, \quad \text{and} \quad \beta_y(z,t) = B_y e^{i(kz-\omega t)}, \\ v(x,t) &= Ve^{i(kz-\omega t)}, \quad \text{and} \quad \beta_x(z,t) = B_x e^{i(kz-\omega t)}, \end{aligned} \tag{29}$$

where (U, V, B_x, B_x) are amplitudes. Substitution of these wave forms into the homogeneous form of Eq. (6) yields the following algebraic eigenproblems:

$$\begin{aligned} \begin{bmatrix} k_{22}^2 GAk^2 & -ik_{22}^2 GAk \\ ik_{22}^2 GAk & EI_{xx}k^2 + k_{22}^2 GA \end{bmatrix} \begin{Bmatrix} V \\ B_y \end{Bmatrix} &= \rho\omega^2 \begin{bmatrix} A & \cdot \\ \cdot & I_{xx} \end{bmatrix} \begin{Bmatrix} V \\ B_y \end{Bmatrix}, \\ \begin{bmatrix} k_{11}^2 GAk^2 & -ik_{11}^2 GAk \\ ik_{11}^2 GAk & EI_{yy}k^2 + k_{11}^2 GA \end{bmatrix} \begin{Bmatrix} U \\ B_x \end{Bmatrix} &= \rho\omega^2 \begin{bmatrix} A & \cdot \\ \cdot & I_{yy} \end{bmatrix} \begin{Bmatrix} U \\ B_x \end{Bmatrix}. \end{aligned} \tag{30}$$

For each eigenproblem, there are two branches in the frequency spectra. The lowest defines the natural frequency for flexural motion as a function of k. The other branch pertains to the thickness-shear vibrations.

Of particular interest are the frequencies of thickness-shear modes of infinitely long wave lengths where $k = 0$. These frequencies for motions in the x-z and y-z planes are

$$\omega^2 = \frac{k_{22}^2 GA}{\rho I_{xx}} \quad \text{and} \quad \omega^2 = \frac{k_{11}^2 GA}{\rho I_{yy}} \tag{31a}$$

so that

$$k_{22}^2 = \frac{\rho I_{xx}}{GA}\omega^2 \quad \text{and} \quad k_{11}^2 = \frac{\rho I_{yy}}{GA}\omega^2. \tag{31b}$$

Shear correction factors on a dynamic basis are based on Eq. (31b), where ω^2 are the three-dimensional thickness-shear frequencies from algebraic eigensystem (28b). It is important to extract the appropriate thickness-shear frequencies from system (28b), as the eigensolution yields a rather vast spectra. A visual examination of all vibration modes will easily reveal which ones are the lowest order thickness-shear modes. Some examples of these infinitely long wave length thickness-shear modes are shown in Fig. 3.[4]

[4] Thickness-shear modes for rectangle and ellipse sections are omitted in Fig. 3, because they are identical to Saint-Venant warpages shown in Fig. 1, for these sections.

Hutchinson (2001) presented another method for shear correction factors. He used a Hellinger–Reissner variational principle to derive equations of motion that may be considered as the "best" equivalent Timoshenko-type equations. Upon invoking a harmonic waveform, he is then able to compare this solution with that based on the Timoshenko beam equations to produce formulas for shear correction factors. In his Hellinger–Reissner functional, independent assumptions of both stress and displacement fields were used. For displacements, a field according to elementary beam theory was adopted, which is essentially the primal field of Saint-Venant flexure – i.e., $\mathbf{\Phi_{sv2}}$ in Eq. (9b). For transverse shear stresses, those of Saint-Venant flexure for a tip loaded cantilevered beam were used. Therefore, this variational approach may be considered as a best (or, alternatively, a least-squares residual) fit of three-dimensional information into a system of one-dimensional equations of motion that account for transverse shear deformation.

Hutchinson dealt mainly with doubly symmetric cross-sections. His formulas for elliptical and rectangular sections in our notation are, respectively,

$$k_{22}^2 = \frac{6(1+3\phi^2)(1+\nu)^2}{20\phi^4 + 8\phi^2 + \nu(37\phi^4 + 10\phi^2 + 1) + \nu^2(17\phi^4 + 2\phi^2 - 3)} \tag{32}$$

and

$$k_{22}^2 = \frac{1+\nu}{1.2+\nu-f} \quad \text{where} \quad f = \frac{18\nu^2}{(1+\nu)\phi^5}\sum_{n=1}^{\infty}\frac{n\pi\phi - \tanh(n\pi\phi)}{(n\pi)^5}, \tag{33}$$

where ν is the Poisson's ratio, and $\phi = b/a$ is the aspect ratio (see, Fig. 4). There are misgivings with these formulas. In Figs. 3 and 4 of Hutchinson (2001), negative shear correction factors are shown when either or both Poisson's and aspect ratios exceed certain limits. One culprit is the term f in the denominator of Eq. (33). This issue was also raised by Stephen (2001). Negative values are not plausible for they violate the first law of thermodynamics in work and energy expressions. For Poisson's ratio $\nu = 0.3$, Hutchinson's factor without the f term is $k_{22}^2 = 0.867$. Stephen (1980) independently obtained essentially the same formula as Hutchinson. With his formula, the same value of $k_{22}^2 = 0.867$ is obtained for deep cross-sections. Stephen's formula was also capable of negative factors, particularly for shallow or flat cross-sections. However, he cautioned against using the formula for anything but deep cross-sections. Note that for $\phi \geqslant 1$ (*deep sections*), we have $(\phi, f) = \{(1, 0.018), (2, 0.0003), (3, 0.00003), \ldots\}$, and f is minimally affected by ϕ.

For *shallow* cross-sections $(\phi < 1)$, f is magnified as ϕ^5 occurs in the denominator. This produces negative correction factors as well as seemingly unrealistic values. For our rectangular cross-sections (cf., Table 3), we will use a shear correction factor as given by Eq. (33) for $\phi > 1$. However, for $\phi < 1$, we will use a shear correction factor without f, thus rendering it independent of aspect ratio ϕ. Such a factor *sans* f will be dubbed the *ad hoc* Hutchinson factor. There is some merit in this choice given that both Hutchinson and Cowper used the same shear stress distribution in their derivations. Cowper obtained factors independent of aspect ratio, so that we anticipate that *ad hoc* Hutchinson factors will acquit themselves well in comparison with three-dimensional results. This will be seen in a subsequent section. In our examples on the ellipse with Poisson's ratio $\nu = 0.3$, formula (32) does not give negative values for all aspect ratios which we are considering. Hence, we will use it as shown.

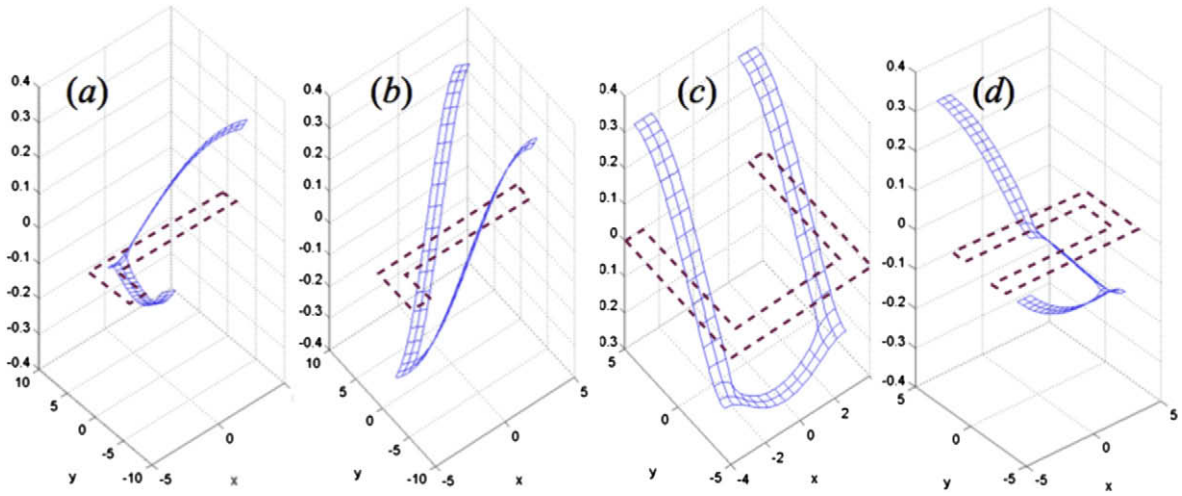

Fig. 3. Examples of thickness-shear vibration modes corresponding to infinitely long waves: (a, b) angle section No. 1, and (c, d) channel section No. 1.

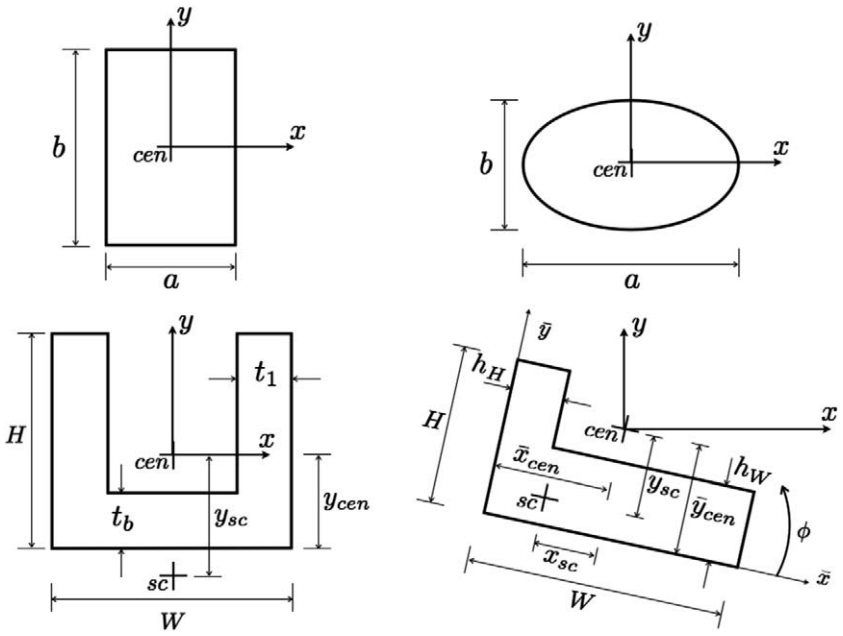

Fig. 4. Geometries and measures for various cross-sections.

5. Examples of cross-sections

Shear correction factors for four cross-sections are presented in tabular form in this section, viz., (1) rectangle, (2) ellipse, (3) channel, and (4) angle. Their geometries are defined in Fig. 4. For the rectangle and ellipse, the aspect ratio $\phi = b/a$ is the basic parameter; only the correction factor k_{22}^2 need to be listed, as k_{11}^2 is given under the inverse aspect ratio. For the channel and angle, their geometric parameters and locations of the centroid and shear centers are tabulated in Tables 1 and 2. Shear correction factors based on (1) Saint-Venant weighted-average warpage angle, (2) vibration method, (3) Hutchinson's method (for rectangles and ellipses only), (4) Renton's method, and (5) directional shear energy are tabulated in Tables 3–6. For directional shear energy, the percentage of the total shear energy in the direction of the transverse force appears in parentheses. All factors presume a coordinate system with the origin at the centroid and (x,y) coordinate axes parallel to the principal bending axes. It is furthermore assumed that all transverse shear forces pass through the shear center of the cross-section. The performance of these correction factors for both static and free vibration responses is given in the next section.

Table 1
Geometry of channel cross-sections.

Section	H	W	t_1	t_b	y_{cen}	y_{sc}
1	8.5	7.0	1.0	1.0	3.3977	6.2954
2	8.5	8.0	2.0	1.0	3.8553	6.5647
3	8.5	10.0	4.0	1.0	4.1429	5.5234
4	9.0	7.0	1.0	2.0	3.2500	5.1541
5	10.0	7.0	1.0	4.0	3.5000	3.4638
6	9.0	8.0	2.0	2.0	3.8636	5.7830
7	10.0	8.0	2.0	4.0	4.1429	4.3136
8	9.0	10.0	4.0	2.0	4.3158	5.1526
9	10.0	10.0	4.0	4.0	4.7273	4.1798

Table 2
Geometry of angle cross-sections.

Section	H	W	h_W	h_H	$\bar{x}_{cen}$	$\bar{y}_{cen}$	ϕ	x_{sc}	y_{sc}
1	10	10	1.0	1.0	2.8684	2.8684	45.00	3.3062	·
2	10	10	2.0	2.0	3.2222	3.2222	45.00	2.9691	·
3	10	10	3.0	3.0	3.5588	3.5588	45.00	2.5180	·
4	6	10	1.0	1.0	3.5000	1.5000	19.64	2.3370	2.9109
5	6	10	2.0	2.0	3.8571	1.8571	17.77	1.8704	1.5372
6	6	10	3.0	3.0	4.1923	2.1923	15.09	1.2658	1.0580
7	6	10	2.0	1.0	4.2500	1.5000	12.53	2.4643	1.2248
8	6	10	3.0	2.0	4.3333	2.0000	12.39	1.4133	1.0170
9	6	10	3.0	1.0	4.5909	1.7727	8.02	1.4400	0.7257

6. Performance of correction factors

The potency of Timoshenko shear correction factors is measured by their capacity to replicate three-dimensional results. We will make measurements with static and vibration data by comparing (1) centroidal axis deflections in a tip-loaded cantilevered beam and (2) normalized frequencies of harmonic waves, where the lowest thickness-shear frequency ω_s is used for normalization. In all cases, Poisson's ratio $\nu = 0.3$.

In the Saint-Venant solution, the warpage functions depicted the three-dimensional or point-wise representation of shear effects. These deformation patterns resulted in shear angle γ_x or γ_y of Eq. (21) or (22), which led to a weighted-average fit of a fully clamped condition. Adding shear deflection based on this angle as a rigid body rotation onto the Saint-Venant centroidal deflection with boundary conditions (8) gives Eq. (23); this deflection curve is identical to that by Timoshenko beam theory. Since this shear angle is inversely proportional to the correction factor, then all other correction factors can be judged according to its relation to it. This factor, we noted, is also the same as that by Cowper (1966, 1968) and Mason and Herrmann (1968). Any shear correction factor of lower value, over-corrects for shear, and conversely, and one that is higher under-corrects.

On this elastostatic basis, all factors for rectangular and elliptical cross-sections in Tables 3 and 4 over correct for shear except for Hutchinson (2001), which under corrects. For a rectangle of aspect ratio $b/a = 10$ and 0.1, values of $k^2 = 0.833$ and 0.179 were obtained by El Fatmi and Zenzri (2004). These are in agreement with Renton's values in Table 3 and suggest that their beam theory is predicated on equality of shear strain energies. For channel and angle cross-sections – factors for which are given in Tables 5 and 6 – the thickness-shear and Renton's energy methods over-correct, and directional energy method under-corrects (there are no factors by Hutchinson's method). It should be remembered that this assessment of correction factors for static loading conditions is based on a tip loaded cantilevered beam. Other loadings may not follow these guidelines. However, it is known that the transverse shear stress distribution for a uniformly loaded beam by three-dimensional theory, i.e., by the Almansi-Michell problem, is the same as Saint-Venant flexure except that now it varies linearly with z. Cowper (1966) intimated that, for loadings that do not vary rapidly with z, shear correction factors based on a tip loaded cantilevered beam should be suitable.

Table 3
Shear correction factors for rectangular cross-sections ($\nu = 0.3$).

b/a	Thickness-shear				
	Saint-Venant	Vibration	Hutchinson	Renton	Directional shear energy
10	0.850	0.822	0.867	0.833	0.833 (100%)
8	0.850	0.822	0.867	0.833	0.833 (100%)
5	0.850	0.822	0.867	0.833	0.833 (100%)
3	0.850	0.822	0.867	0.833	0.833 (100%)
2	0.850	0.822	0.867	0.833	0.833 (100%)
1.5	0.850	0.822	0.869	0.832	0.832 (≈100%)
1 (square)	0.850	0.822	0.877	0.828	0.829 (99.9%)
0.667	0.850	0.822	0.929	0.813	0.820 (99.1%)
0.500	0.850	0.822	1.126	0.784	0.807 (97.2%)
0.333	0.850	0.822	-3.026	0.694	0.777 (89.3%)
0.200	0.850	0.822	-0.089	0.478	0.720 (66.4%)
0.125	0.850	0.822	-0.012	0.258	0.648 (39.9%)
0.100	0.850	0.822	-0.005	0.179	0.607 (29.5%)

For $b/a < 1$, Hutchinson's *ad hoc* shear correction factor is 0.867.

Table 4
Shear correction factors for elliptical cross-sections ($\nu = 0.3$).

b/a	Thickness-shear				
	Saint-Venant	Vibration	Hutchinson	Renton	Directional shear energy
8	0.915	0.889	0.932	0.899	0.900 (99.9%)
5	0.914	0.888	0.932	0.898	0.900 (99.7%)
3	0.912	0.884	0.931	0.894	0.900 (99.3%)
2.5	0.910	0.882	0.931	0.891	0.900 (99.0%)
2	0.907	0.878	0.930	0.886	0.900 (98.4%)
1.5	0.902	0.869	0.929	0.876	0.899 (97.3%)
1 (circle)	0.886	0.847	0.925	0.851	0.899 (94.6%)
0.667	0.859	0.812	0.912	0.806	0.897 (89.9%)
0.500	0.828	0.781	0.911	0.758	0.894 (84.7%)
0.400	0.792	0.756	0.904	0.709	0.892 (79.4%)
0.333	0.757	0.736	0.897	0.659	0.891 (74.0%)
0.200	0.612	0.457	0.858	0.476	0.887 (53.7%)
0.125	0.419	0.334	0.780	0.286	0.885 (32.4%)

Table 5
Shear correction factors for channel cross-sections ($\nu = 0.3$).

b/a	Thickness-shear			
	Saint-Venant	Vibration	Renton	Directional shear energy
About y-axis				
1	0.645	0.610	0.624	0.668 (93.5%)
2	0.756	0.718	0.731	0.764 (95.6%)
3	0.831	0.801	0.804	0.813 (98.8%)
4	0.554	0.524	0.539	0.574 (94.0%)
5	0.541	0.492	0.533	0.569 (93.8%)
6	0.695	0.657	0.637	0.707 (95.2%)
7	0.677	0.634	0.662	0.696 (95.1%)
8	0.811	0.779	0.785	0.798 (98.4%)
9	0.805	0.771	0.783	0.797 (98.3%)
About x-axis				
1	0.179	0.164	0.177	0.297 (59.7%)
2	0.145	0.134	0.143	0.206 (69.2%)
3	0.143	0.124	0.142	0.199 (71.1%)
4	0.236	0.200	0.236	0.451 (52.4%)
5	0.321	0.238	0.328	0.598 (54.9%)
6	0.209	0.185	0.207	0.338 (61.2%)
7	0.298	0.243	0.300	0.503 (59.6%)
8	0.212	0.180	0.209	0.312 (67.1%)
9	0.317	0.258	0.315	0.470 (67.1%)

Table 6
Angle cross-sections: correction factors in principle directions ($\nu = 0.3$).

b/a	Thickness-shear			
	Saint-Venant	Vibration	Renton	Directional shear energy
About y-axis				
1	0.442	0.422	0.439	0.810 (54.2%)
2	0.473	0.458	0.470	0.793 (59.2%)
3	0.558	0.521	0.514	0.785 (65.4%)
4	0.532	0.515	0.527	0.685 (76.9%)
5	0.584	0.563	0.578	0.695 (82.2%)
6	0.656	0.629	0.649	0.722 (89.8%)
7	0.656	0.625	0.650	0.764 (85.0%)
8	0.682	0.657	0.675	0.749 (90.1%)
9	0.743	0.716	0.735	0.794 (92.5%)
About x-axis				
1	0.442	0.433	0.433	0.850 (50.9%)
2	0.473	0.461	0.483	0.886 (54.5%)
3	0.517	0.498	0.565	0.914 (61.9%)
4	0.327	0.305	0.327	0.455 (71.8%)
5	0.426	0.363	0.421	0.548 (78.8%)
6	0.594	0.481	0.575	0.670 (85.6%)
7	0.304	0.244	0.288	0.363 (79.2%)
8	0.528	0.381	0.501	0.600 (83.6%)
9	0.473	0.283	0.433	0.510 (85.0%)

For vibration, frequencies of a sinusoidal wave form (27) given by three-dimensional elasticity, i.e., Taweel et al. (2000), are compared with all Timoshenko beam results. The important parameters are wave number k and ratio D/λ of depth to wave length, where $k = \pi/\lambda$. Comparative data are presented in terms of percentage difference between elasticity and Timoshenko beam data as a function of D/λ, where this percentage difference is defined as

$$\%\text{-difference} = \frac{\omega_{3D} - \omega_{Timo}}{\omega_{3D}} \times 100. \tag{34}$$

Two different cross-sections for each type of beam were considered, where vibrations about both principal axes were evaluated.

For rectangular cross-sectional shapes, aspect ratios $b/a = 2$ and 8 and their reciprocals were considered and the comparisons are shown in Fig. 5(a–d). Observe in all the plots that the results by *ad hoc* Hutchinson factor show the least departure from elasticity, followed by those of the Saint-Venant factor. In vibrations about the *shallow* direction – cf., Fig. 5(a and b) –, the frequencies in the case $b/a = 8$ were off by less than 3% except for those of Renton and directional shear energy, which exceeded 10% difference at $D/\lambda = 1$. For vibrations about an axis perpendicular to the *deep* direction – cf., Fig. 5(c and d) –, deviations from three-dimensional data are quite small and smaller in comparison to that about the *shallow* direction. While Hutchinson method yielded the most superior result, we need to also acknowledge that for the worst performing shear correction factor – i.e., thickness-shear –, the frequencies were only off by 2% at $D/\lambda = 1$. On this basis, any of the shear correction factors qualifies as eminently suitable for providing acceptable frequencies. No plot of the frequency spectra is shown here, as all spectral curves would be piled on top of each other in such a figure.

For elliptical cross-sections, aspect ratios $b/a = 2$ and 8 and their reciprocals were considered. The results are quite similar to those for the rectangle in the *deep* direction – see, Fig. 6(c, d). Again, the Hutchinson factor acted the best followed by that by Saint-Venant flexure. For vibrations about the *shallow* direction, Fig. 6 (a and b), moderately greater discrepancies were seen *vis-a-vis* the rectangle. For $b/a = 1/8$, it appears that for %-differences less than 5%, the range stops around $D/\lambda = 0.25$. Here, it is again seen that Timoshenko beam results can be quite accurate even up to $D/\lambda = 1$.

For the channel, cross-sections 1 and 9 in Table 1 were considered to provide a contrast based on the widths of their leg and bridge portions. For cross-section 1, which is a thin section, flexural frequency spectra for vibrations about the y-axis are shown in Fig. 7, where a complete lack of agreement between Timoshenko beam and three-dimensional elasticity data is apparent. There is an absence of a pure flexure mode in the three-dimensional elasticity data, as seen in Fig. 8 for $D/\lambda = 0.05$, where an in–plane rotational pattern indicates a significant torsional component even though a strong flexural action is also present. For this cross-section, the flexural and torsional rigidities are $EI_{yy} = 164.83$ and $GJ = 2.81$, a low ratio of GJ/EI_{yy}. Without a pure elasticity flexural mode, a meaningful comparison of Timoshenko beam data is not possible.

Frequency spectra for channel Section 1 in flexural vibrations about the x-axis – i.e., the other principal axis – are shown in Fig. 9a, and comparative data appear in Fig. 9c. As can be seen, agreement of Timoshenko data occurs in a very limited range of D/λ. Large discrepancies appear to begin at $D/\lambda = 0.18$. For cross-section 9, a similar conclusion can be drawn on vibrations about the y-axis. No meaningful comparison is possible as a pure flexural mode is not present. A bending-torsional mode appears immediately after D/λ departs from the origin, even though the GJ/EI_{xx} ratio is much higher, i.e, $EI_{yy} = 829.33$ vs. $GJ = 174.63$. It appears that for channel cross-sections, vibrations about the y-axis consist of bending-torsion motions regardless of their GJ/EI_{xx} ratios. Data for vibration about the x-axis are given in Fig. 9b and d. In Fig. 9b showing the flexural spectra, the departure of Timoshenko beam data does not occur until $D/\lambda = 0.65$. In Fig. 9d, all shear correction factors appear to be able to replicate frequencies to within 1% accuracy up to $D/\lambda = 0.5$. The thicker legs of this cross-section extended the range of Timoshenko beam theory well beyond that with thin legs.

Angle cross-sections 1 and 6 of Table 2 were considered as these two sections also contrasted thin legs versus thick legs. Moreover, cross-section 6 is completely non-symmetric. There is no pure flexural vibration about the x-axis in cross-section 1, as bending and torsional behaviors occur at the outset of wave $k \neq 0$. This behavior is similar to that in the thin walled channel. For vibration about the y-axis, the flexural spectra are shown in Fig. 10a that shows the elasticity and Timoshenko beam results parting ways in the vicinity of $D/\lambda = 0.15$. A plot of the percentage differences is given in Fig. 10c. While the errors of classical theory are nominally higher

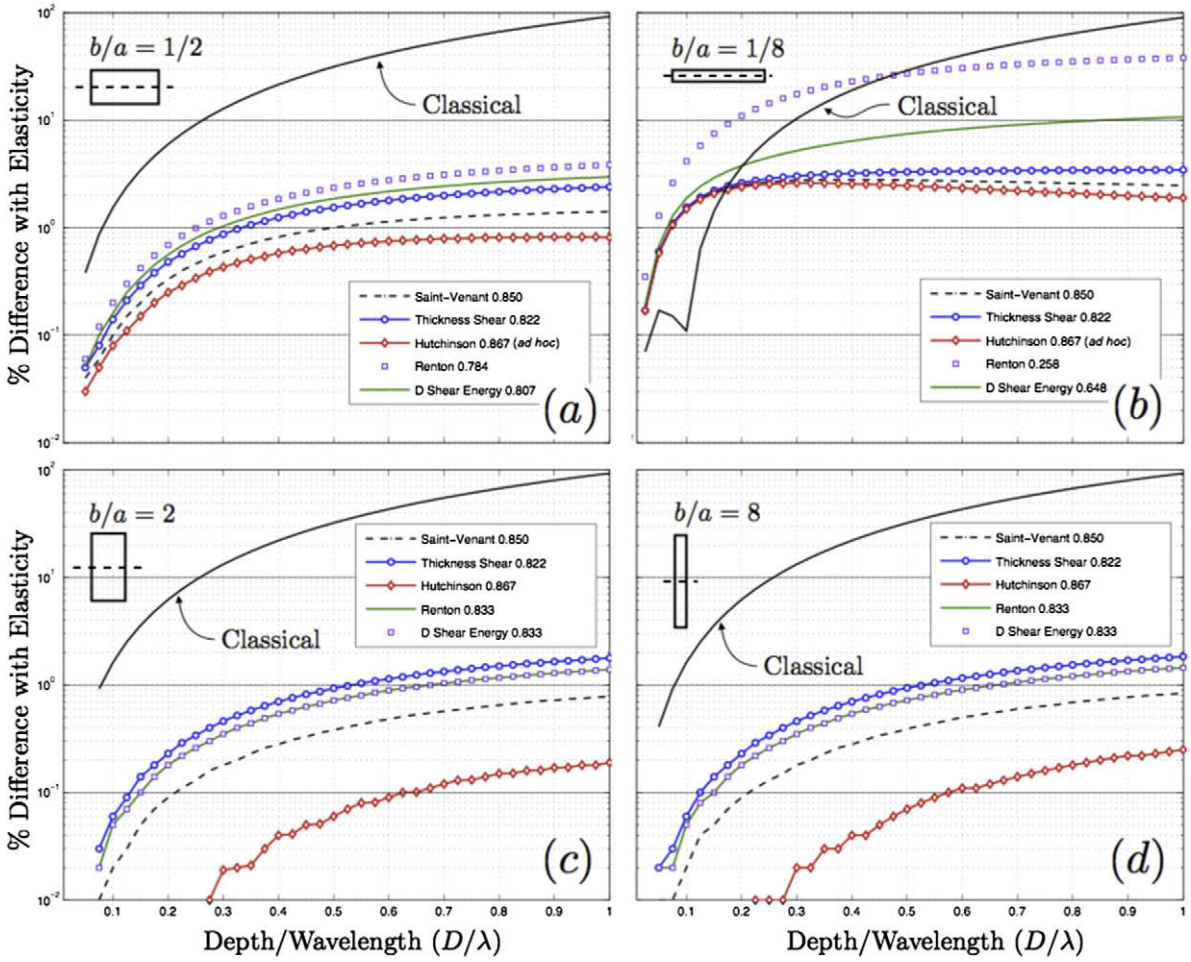

Fig. 5. Comparison of frequencies of rectangular cross-sections: shallow sections (a, b); deep sections (c, d).

up to $D/\lambda = 0.15$, the difference is almost inconsequential as Timoshenko beam theory only provides for a minimum improvement.

For cross-section 6, the unnormalized elasticity spectral data are presented in Fig. 11. We see that there is one flexural mode (about the y-axis) and two coupled bending-torsion modes with respect to the other principal axis. These labels of the spectra are based on inspections of their modal patterns. The flexural spectra of both elasticity and Timoshenko beam modes are shown in Fig. 10b. Good agreement is observed up to $D/\lambda \approx 0.3$. The percentage differences of the Timoshenko beam results with elasticity are shown in Fig. 10d, where Timoshenko data exceed 5% difference at roughly $D/\lambda \approx 0.3$. The spectra for vibrations about the other (second) principal axis are shown in Fig. 12. Here, an unusual phenomenon is occuring. The elasticity frequency spectrum is higher than the Timoshenko beam spectra. In Fig. 11, we identified the first mode as coupled bending-torsional behavior. For this cross-section, $EI_{xx} = 71.96$ and $GJ = 40.69$[5]; the presence of considerable torsional rigidity is reflected in a higher frequency for the fundamental (coupled bending–torsion) elasticity mode. The sum of flexural and shear rigidities in Timoshenko beam is less than the amount of flexure and torsion. In Fig. 13, a three-dimensional elasticity modal pattern is given to show this coupled behavior. When a pure flexural mode is pre-empted, a meaningful comparison of Timoshenko beam data is not possible.

In summary, we see that Timoshenko beam theory works well for rectangular and elliptical cross-sections for factors by Hutchinson's and Cowper's methods. Renton's and directional shear methods work well for deep cross-section; but when the geometry becomes shallow, there is a substantial decline in their effectiveness. Directional shear energy factors are able to improve upon Renton's factors, but their overall effectiveness deserves to be explored further. For channel and angle cross-sections, the three-dimensional bending-torsion coupling phenomenon with respect to one principal bending axes precludes any possibility of Timoshenko type theory capturing this behavior. Timoshenko beam theory can only capture the bending behavior about the other principal axis. Moreover, the range of application of Timoshenko beam theory is quite restrictive for such cross-sections *vis-a-vis* rectangles and ellipses.

7. The issue of principal shear axes

Schramm et al. (1994) extended Renton's concept of equating comparable energies to determine shear correction factors for non-symmetrical cross-sections. They introduced principal shear axes that were not coincident with the principal bending axes in their formulation. An examination of the Saint-Venant flexure solution will dissuade this concept. It shows deflection of the centroidal axis lying in the same plane as the transverse load; there is no displacement normal to this plane. If Timoshenko beam constitutive relations are based on non-coincident principal bending and shear axes, then a lateral or sidesway displacement will be admitted. Such behavior precludes any opportunity for Timoshenko beam theory to ever replicate linear three-dimensional elasticity results.

[5] For cross-section 1, $EI_{xx} = 73.43$ and $GJ = 2.39$.

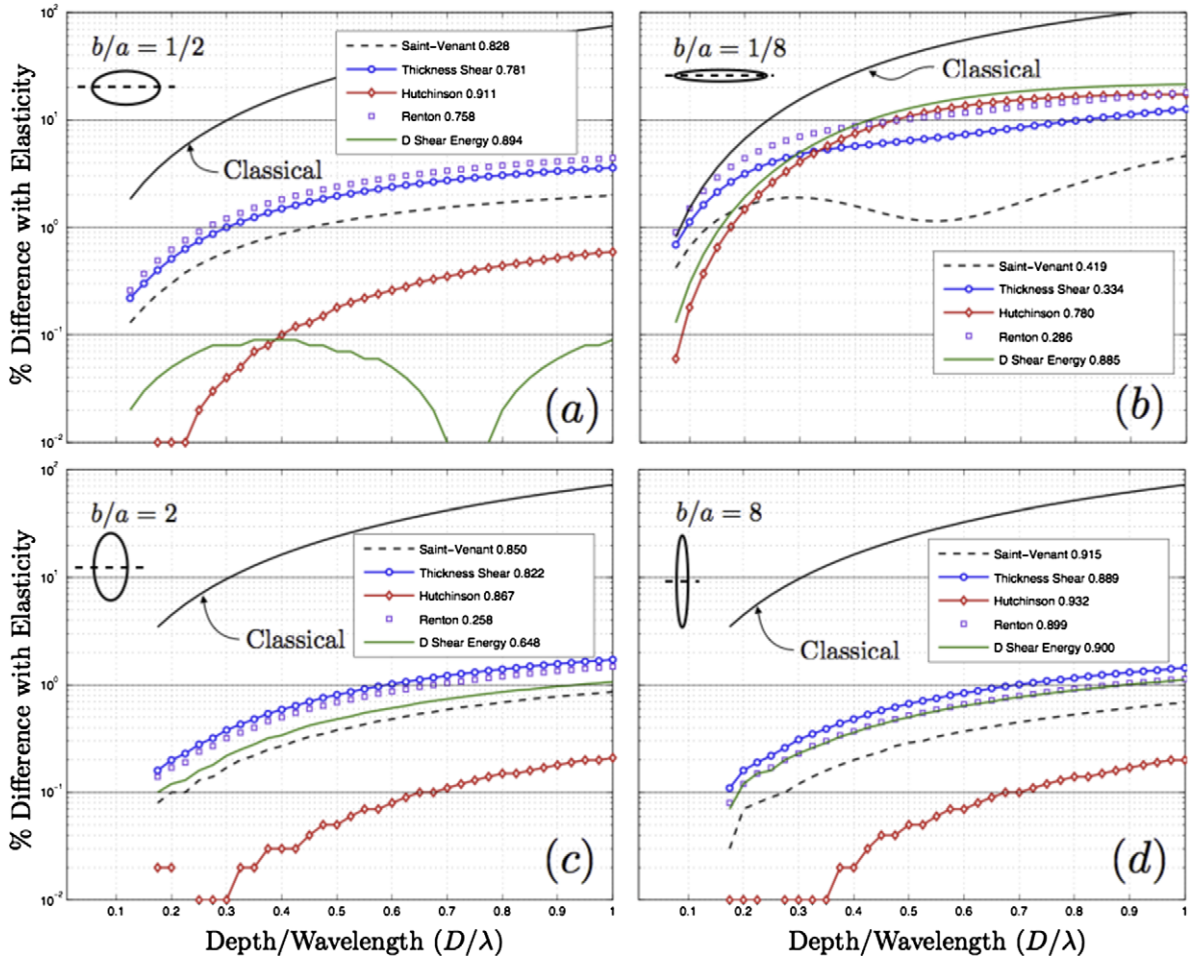

Fig. 6. Comparison of frequencies of elliptic cross-sections: ahallow sections (a, b); deep sections (c, d).

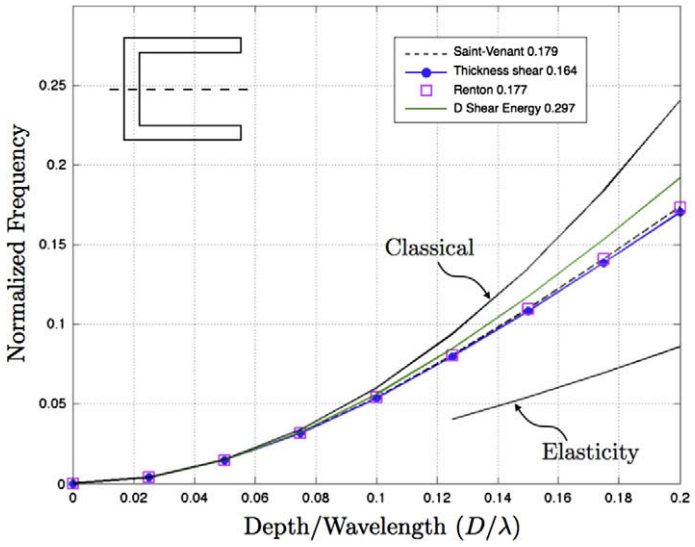

Fig. 7. Flexural spectra for channel cross-section No. 1 about *y*-axis.

Schramm et al's method for the Timoshenko beam shear correction factors for a non-symmetric cross-section involves the following expressions of the shear angles in terms of the transverse forces:

$$\gamma_{xz} = \alpha_{xx}\frac{\overline{V}_x}{GA} + \alpha_{xy}\frac{\overline{V}_y}{GA}, \quad \gamma_{yz} = \alpha_{yx}\frac{\overline{V}_x}{GA} + \alpha_{yy}\frac{\overline{V}_y}{GA}, \text{ where } \alpha_{xy} = \alpha_{yx}. \tag{35}$$

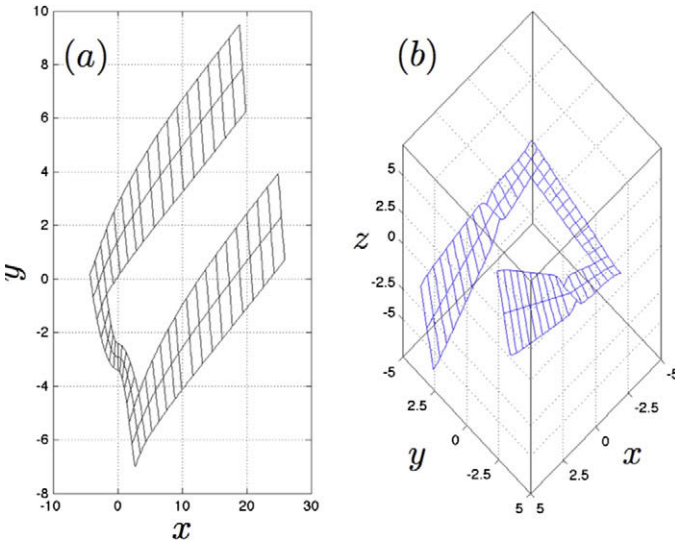

Fig. 8. Mode shape of vibration of channel cross-section No. 1 about y-axis: (a) in–plane and (b) out-of-plane components.

In these expressions, the terms $\overline{V}_i/GA$ denote shear angles; and coefficients α_{ij} are the inverses of the shear correction factors k_{ij}^2. Popescu and Hodges (2000) adopted the same procedure on matching energies in studying beams that were not isotropic. Observe that these shear angle expressions imply the presence of shear forces in both orthogonal directions. The shear strain energy per unit length in terms of these shear angles and their corresponding shear forces has the form

$$U_{sb} = \frac{1}{2}\int_A (\sigma_{xz}\gamma_{xz} + \sigma_{yz}\gamma_{yz})dA = \frac{1}{2}\left[\alpha_{xx}\frac{V_x\overline{V}_x}{GA} + \alpha_{xy}\frac{V_x\overline{V}_y}{GA} + \alpha_{yx}\frac{V_y\overline{V}_x}{GA} + \alpha_{yy}\frac{V_y\overline{V}_y}{GA}\right]. \tag{36}$$

Let us now state the shear strain energy per unit length, U_{se}, by three-dimensional elasticity. Using superscripts x and y to denote stress components of forces in these directions, respectively,

$$\sigma_{xz} = \sigma_{xz}^x + \sigma_{xz}^y \quad \text{and} \quad \sigma_{yz} = \sigma_{yz}^x + \sigma_{yz}^y. \tag{37}$$

We have

$$U_{se} = \frac{1}{2G}\int_A \left[(\sigma_{xz}^x + \sigma_{xz}^y)^2 + (\sigma_{yz}^x + \sigma_{yz}^y)^2\right]dA = U_{se}^{xx} + U_{se}^{yy} + 2U_{se}^{xy}, \tag{38}$$

where

$$U_{se}^{xx} = \frac{1}{2G}\int_A [(\sigma_{xz}^x)^2 + (\sigma_{yz}^x)^2]\,dA, \quad U_{se}^{yy} = \frac{1}{2G}\int_A [(\sigma_{xz}^y)^2 + (\sigma_{yz}^y)^2]\,dA$$
$$U_{se}^{xy} = \frac{1}{2G}\int_A [\sigma_{xz}^x\sigma_{xz}^y + \sigma_{yz}^x\sigma_{yz}^y]\,dA. \tag{39}$$

Schramm et al. equated Eq. (36) to Eq. (38) and matched each shear correction factor to its corresponding energy expression. We paraphrase their results, given by Eqs. (66) to (68) of Schramm et al.'s (1994) paper, as

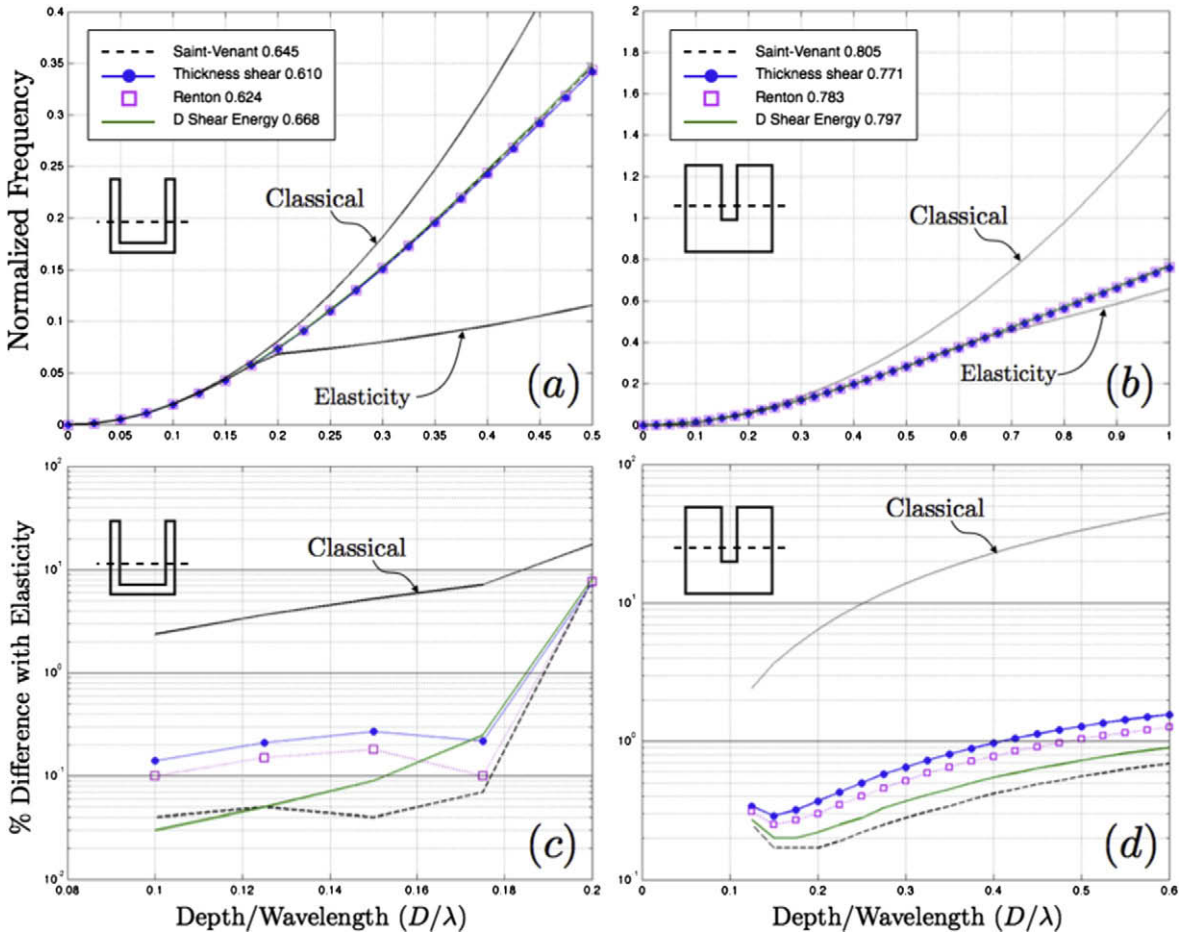

Fig. 9. Flexural spectra about x-axis for channel cross-sections Nos. 1 and 9 (a, b), and their comparison with the elasticity solution (c, d).

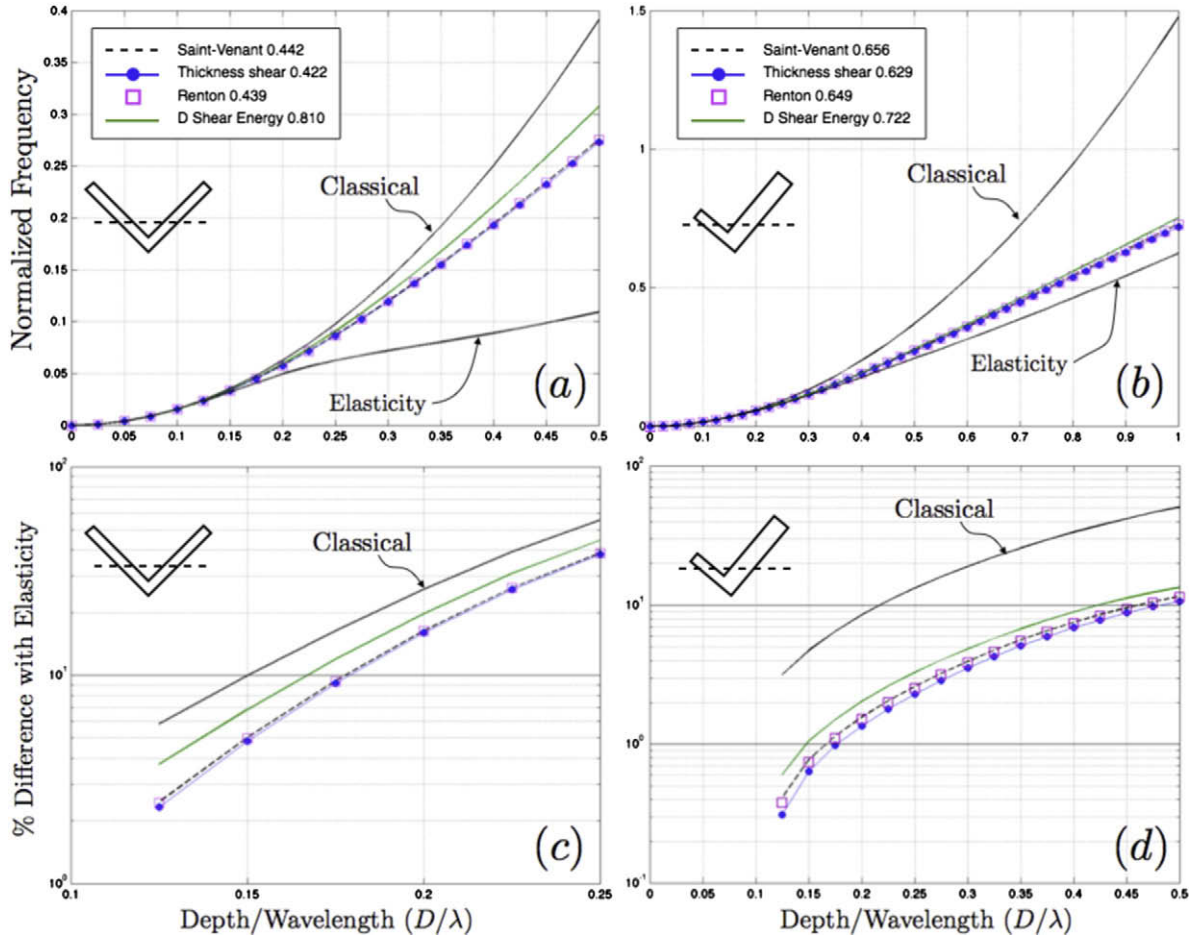

Fig. 10. Flexural spectra about y-axis for angle cross-section No. 1 (a), and their comparison with the elasticity solution (c). Flexural spectra about the first principal bending axis for angle cross-section No. 6 (b), and their comparison with the elasticity solution (d).

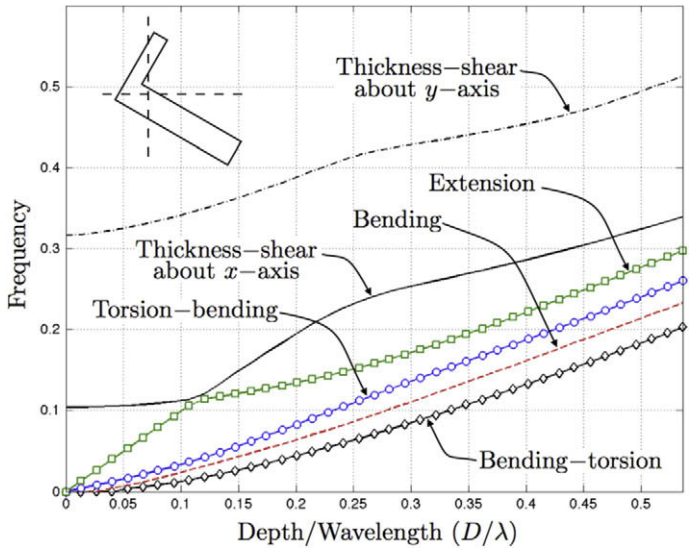

Fig. 11. Three-dimensional spectra for angle cross-section No. 6.

$$\alpha_{xx}=\frac{GA}{V_x\overline{V}_x}U_{se}^{xx},\quad \alpha_{yy}=\frac{GA}{V_y\overline{V}_y}U_{se}^{yy},\quad \alpha_{xy}=\alpha_{yx}=\frac{GA}{V_x\overline{V}_y}U_{se}^{xy}=\frac{GA}{V_y\overline{V}_x}U_{se}^{xy}. \tag{40}$$

Observe that Eqs. (37)–(39) are valid for all coordinate directions, even those parallel to the principal bending axes. Moreover, for a given pair of forces in any two orthogonal directions, strain energy (38) is invariant with respect to coordinate rotation about an axis normal to the cross-section. The shear strain energy is unchanged. If strain energy expression (36), i.e., the right-hand side, is transformed to principal bending axes, then α_{xy} should vanish. This raises a conundrum on the term U_{se}^{xy} in the third equation of (40). It is generally not zero, even when the forces are in the principal bending

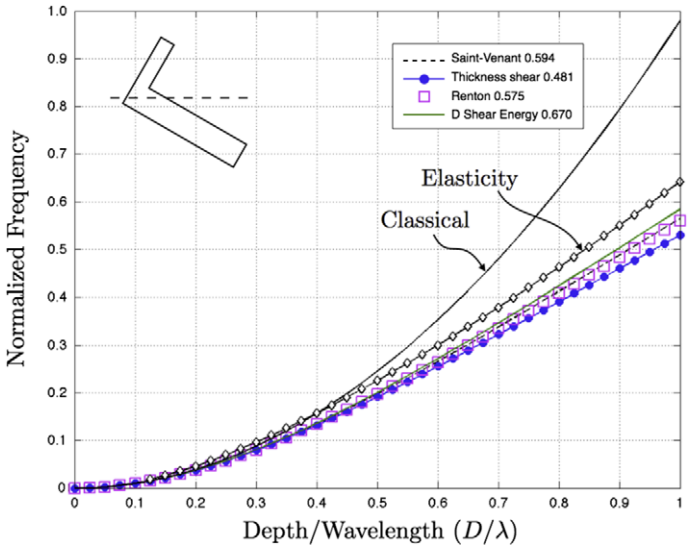

Fig. 12. Flexural spectra about for angle cross-section No. 6 about the second principal bending axis.

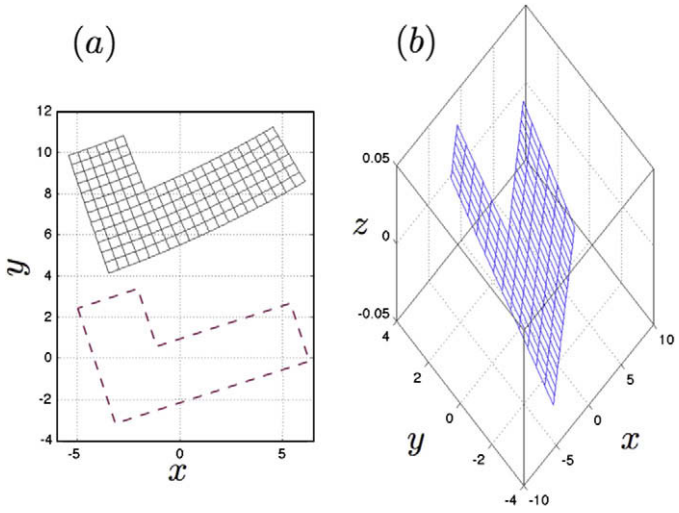

Fig. 13. Mode shape for angle cross-section No. 6 about the second principal bending axis: (a) in-plane and (b) out-of-plane components.

directions. Only for cross-sections possessing at least one plane of structural symmetry, U_{se}^{xy} will vanish in the principal bending directions – a consequence of orthogonality of the shear stress states for the two forces. For unsymmetrical cross-sections, it will not vanish. What Schramm et al. (1994) found, which they dubbed "the principal shear axes," was an alternate set of axes where the two shear stress states evince the aforementioned orthogonality. However, *this is not pertinent to shear correction factors*!

It is not appropriate to begin shear correction calculations with an expression of form (36) consisting of stresses and strains of two force systems. Only a single transverse force at a time can be considered, and it is expedient to adopt a coordinate system oriented in the principal bending directions.[6] Then, the shear correction factors in the principal bending directions are found by two equations, each equivalent to that of Renton (1991):

$$\alpha_{xx} = \frac{GA}{V_x^2} U_{se}^{xx} = \frac{1}{2V_x^2} \int_A [(\sigma_{xz}^x)^2 + (\sigma_{yz}^x)^2]\, dA,$$
$$\alpha_{yy} = \frac{GA}{V_y^2} U_{se}^{yy} = \frac{1}{2V_y^2} \int_A [(\sigma_{xz}^y)^2 + (\sigma_{yz}^y)^2]\, dA. \tag{41}$$

Knowing the shear correction factors in the principal bending directions allows for constitutive relations in any other coordinate system as these factors are components of a second-rank tensor.

8. Concluding remarks

Three-dimensional information and numerical data were central in our discussion to clarify many issues on shear correction factors of Timoshenko beam theory. The displacements (in the SAFE formulation) were vital to the visualization of transverse shear effects in beams of various cross-sections.

In the Saint-Venant flexure solution, we were able to show that the shear deformation warpage was located at the root end. Because the Saint-Venant flexure solution is only unique to within a rigid body motion, we can append another rigid body rotation to this solution. This rigid body motion given by a weighted-average measure of the warpage turns out, in fact, to be the shear angle of Timoshenko beam theory. Moreover, shear correction factors on this basis have the same values as those by Cowper (1966) and Mason and Herrmann (1968). While this analysis is predicated on a tip loaded cantilevered beam, Cowper and others have conjectured persuasively that these shear correction factors should work for other elastostatic loadings, especially ones with only slow variations in the direction of the beam.

For dynamic results, Hutchinson (2001)'s shear correction factors (with our suggested modification for cross-sections with a flat geometry) appeared to have worked exceedingly well for rectangular and elliptical cross-sections. His approach has one conceptual advantage over the long standing method of Mindlin and Deresiewicz (1954), in that the variational formulation offered the "best" equations of motion that accounts for shear deformation. The method of Mindlin and Deresiewicz (1954) makes the Timoshenko beam solution exact at only one wave number, i.e., at $k = 0$. Their trust, most likely, was that major deviations from three-dimensional data would not begin until k is sufficiently into the short wavelength regime.

Our analysis of channel and angle cross-sections revealed an interesting behavior that should caution against blind application

[6] Mason and Herrmann (1968) did not used a coordinate system oriented in the principal bending directions. But only one force was applied at a time and two calculations gave two sets of correction factors, $(\alpha_{ii}^2, \alpha_{ij}^2)$ and $(\alpha_{jj}^2, \alpha_{ji}^2)$. Their procedure allows the symmetry of α_{ij}^2 and α_{ji}^2 to be verified.

of Timoshenko beam theory. These geometries may be said to represent open cross-sections. Three-dimensional data shows that with respect to one of the principal bending axis, coupled bending-torsion modes occur so that any Timoshenko theory without further provisions for torsional behavior will never be able to approximate three-dimensional behavior over any range of wave numbers. Moreover, for these geometries, the range of application of Timoshenko beam theory about the other principal bending axis is abbreviated, vis-a-vis cross-sections of the types such as rectangles and ellipses.

A Timoshenko beam solution employing the shear correction factors herein is an approximation of the *long wavelength solution*, as termed by Ladevéze and Simmonds (1998), where end effects are ignored. Also, while the vibrational plots showed relatively good agreement with three-dimensional data over an extended range, it is noted that periodic boundary conditions employed for the plots do not validate all types of boundary conditions. By an asymptotic analysis of free vibration of a cantilevered beam, Duva and Simmonds (1991) found that the frequency correction due to end effects was of order (H/L), where H is a thickness and L is some wave length measure. This is compared with a $(H/L)^2$ frequency correction due to shear deformation and suggests that end effects may have a potentially greater influence *vis-a-vis* shear. While their analysis based on plane strain conditions is valid for a thin (deep) rectangular cross-section, definitive remarks for all cross-sectional shapes remain open. Many other issues need to be explored for a complete understanding. Inverse decay lengths of flat cross-sections (as opposed to deep cross-sections) have shorter inverse decay lengths as diffusion of end effects can take place three-dimensionally. Thus, even though end effects are modulated by (H/L), the actual correction may still be small. End effects with a greater potential of penetrating into the interior are those in beams composed of extremely low transverse shear stiffnesses, such as seen in fiber-reinforced composites. The influence of boundary conditions is beyond the present scope, but nevertheless it remains to be an important issue.

The determination of shear correction factors for non-symmetrical cross-sections by matching transverse shear energies per unit length was addressed. Here, we showed a nuance, which can easily be overlooked, that only one transverse force can be considered in the calculation of such energies. Using two orthogonal transverse shear forces as Schramm et al. (1994) and Popescu and Hodges (2000) requires the concept of principal shear axes, that is not supported by the Saint-Venant flexure solution.

Lastly, we interject the following thought on shear correction factors for homogeneous, isotropic plates. Mindlin's method (1950) yielded a value of $\pi^2/12$, which is the same as that for rectangular cross-sections. This should not be surprising as for both beams and plates, thickness-shear vibrations involve plane–strain conditions. Reissner's (1947) method required independent fields for transverse and normal stresses in this complementary strain energy expression; his method gave the shear correction factor as 5/6. If the root-end warpage function of the plane–strain flexure solution for beams given by Timoshenko and Goodier (1970, pp. 44–45) were integrated as per our discussion, it should give a shear correction factor appropriate for plate theory, or an alternative to Reissner's. Such an integration gives

$$\frac{1}{k^2} = \frac{3}{20}\left[\frac{8+9\nu}{1+\nu}\right]. \tag{42}$$

For the range of Poisson's ratio $0 \leqslant \nu \leqslant 0.5$, the range of k^2 is $0.833 \geqslant k^2 \geqslant 0.800$. For $\nu = 0.3$, Eq. (42) gives $k^2 = 0.810$ as compared to Reissner's 5/6.

Acknowledgements

The research reported herein was supported by the National Science Foundation under Grant No. CMS-0547670, and in part, by funding from the Faculty Grants Program of UCLA Academic Senate Council on Research. This support is gratefully acknowledged. The opinions expressed in this paper are those of the authors and do not necessarily reflect those of the sponsors.

References

Alpdogan, C., Dong, S.B., Taciroglu, E.T., 2010. A method of analysis for end and transitional effects in anisotropic cylinders. Int. J. Solids Struct. 47, 947–956.
Berdichevsky, V.L., Starosel'skii, L.A., 1983. On the theory of curvilinear Timoshenko-type rods. Prikl. Matem Mekhan. 47, 809–817.
Cowper, G.R., 1966. The shear coefficient in Timoshenko's beam theory. J. Appl. Mech., ASME 33 (2), 335–340.
Cowper, G.R., 1968. On the accuracy of Timoshenko's beam theory. J. Eng. Mech. Div., ASCE 94 (EM6), 1447–1453.
Dong, S.B., Kosmatka, J.B., Lin, H.C., 2001. On Saint-Venant's problem for an inhomogeneous, anisotropic cylinder – Part I: methodology for Saint-Venant solutions. J. Appl. Mech., ASME 68 (3), 376–381.
Duva, J.M., Simmonds, J.G., 1991. The usefulness of elementary theory for the linear vibrations of layered, orthotropic elastic beams and corrections due to two-dimensional end effects. J. Appl. Mech., ASME 58 (1), 175–180.
El Fatmi, R., Zenzri, H., 2002. On the structural behavior and the Saint-Venant solution in the exact beam theory: application to laminated composite beams. Comput. Struct. 80 (16-17), 1441–1456.
El Fatmi, R., Zenzri, H., 2004. A numerical method for the exact elastic beam theory: applications to homogeneous and composite beams. Int. J. Solids Struct. 41, 2521–2537.
El Fatmi, R., 2007a. Non-uniform warping including the effects of torsion and shear forces. Part I: a general beam theory. Int. J. Solids Struct. 44, 5912–5929.
El Fatmi, R., 2007b. Non-uniform warping including the effects of torsion and shear forces. Part II: analytical and numerical applications. Int. J. Solids Struct. 44, 5930–5952.
Gruttmann, F., Wagner, W., 2001. Shear correction factors in Timoshenko's beam theory for arbitrary shaped cross-sections. Comput. Mech. 27, 199–207.
Hutchinson, J.R., 2001. Shear coefficients for Timoshenko beam theory. J. Appl. Mech., ASME 68 (1), 87–92.
Kosmatka, J.B., Dong, S.B., 1991. Saint-Venant solutions for prismatic anisotropic beams. Int. J. Solids Struct. 28 (7), 917–938.
Kosmatka, J.B., Dong, S.B., Lin, H.C., 2001. On Saint-Venant's problem for an inhomogeneous, anisotropic cylinder – Part II: cross-sectional properties. J. Appl. Mech., ASME 68 (3), 382–391.
Ladevéze, P., Simmonds, J., 1998. New concepts for linear beam theory with arbitrary geometry and loading. Eur. J. Mech. A/Solids 17 (3), 377–402.
Ladevéze, P., Sanchez, P., Simmonds, J., 2001. On application of the exact theory of elastic beams. In: Durban, Girolo, Simmonds (Eds.), Advances in the Mechanics of Plates and Shells. Kluwer Academic Publishers.
Lin, H.C., Dong, S.B., Kosmatka, J.B., 2001. Saint-Venant's problem for an inhomogeneous, anisotropic cylinder – Part III: end effects. J. Appl. Mech., ASME 68 (3), 392–398.
Lin, H.C., Dong, S.B., 2006. On the Almansi–Michell problems for an inhomogeneous, anisotropic cylinder. J. Mech. 22 (1), 51–57.
Mason Jr., W.E., Herrmann, L.R., 1968. Elastic shear analysis of general prismatic beams. J. Eng. Mech. Div., ASCE 94 (EM4), 965–983.
Mindlin, R.D., 1951. Influence of rotatory inertia and shear on flexural motions of isotropic, elastic plates. J. Appl. Mech., ASME 18, 31–38.
Mindlin, R.D., Deresiewicz, H., 1954. Timoshenko's shear coefficient for flexural vibrations of beams. In: Proceedings of the 2nd US National Congress of Applied Mechanics 175-178.
Popescu, B., Hodges, D.H., 2000. On asymptotically correct Timoshenko-like anisotropic beam theory. Int. J. Solids Struct. 37, 535–558.
Reissner, E., 1945. The effect of transverse shear deformation on bending of elastic plates. J. Appl. Mech., ASME 67, A69–A77.
Reissner, E., 1947. On bending of elastic plates. Quart. Appl. Math. 5, 55–68.
Renton, J.D., 1991. Generalized beam theory applied to shear stiffness. Int. J. Solids Struct. 27 (15), 1955–1967.
Schramm, U., Kitis, L., Kang, W., Pilkey, W.D., 1994. On the shear deformation coefficient in beam theory. Fin. Elem. Anal. Des. 16, 141–162.
Stephen, N.G., 1980. Timoshenko's shear coefficient from a beam subjected to gravity loading. J. Appl. Mech., ASME 47 (1), 121–127.
Stephen, N.G., 2001. Discussion of Hutchinson's paper shear coefficients for Timoshenko beam theory. J. Appl. Mech., ASME 68 (6), 959–960.
Taweel, H., Dong, S.B., Kazic, M., 2000. Wave reflection from the free end of a cylinder with and arbitrary cross-section. Int. J. Solids Struct. 37, 1701–1726.
Timoshenko, S.P., 1921. On the correction for shear of the differential equation for transverse vibrations of prismatic beams. Philos. Mag. 41, 744–746.
Timoshenko, S.P., 1922. On the transverse vibrations of bars of uniform cross-sections. Philos. Mag. 43, 125–131.
Timoshenko, S.P., Goodier, J.N., 1970. Theory of Elasticity, third ed. McGraw-Hill, New York. pp. 44–45.
Tolf, G., 1985. Saint-Venant bending of an orthotropic beam. Comput. Struct. 4, 1–14.
Wörndle, R., 1982. Calculation of the cross-section properties and the shear stresses of composite rotor blades. Vertica 6, 111–129.